

High CD8 T cell receptor clonality and altered CDR3 properties are associated with elevated isolevuglandins in adipose tissue during diet-induced obesity

Wyatt J. McDonnell¹⁻³, John R. Koethe^{2,4,5}, Simon A. Mallal^{1,2,4,6}, Mark A. Pilkinton^{2,4,5}, Annet Kirabo⁷, Magdalene K. Ameka⁸, Matthew A. Cottam⁸, Alyssa H. Hasty^{5,8}, and Arion J. Kennedy^{8*}

¹ Department of Pathology, Microbiology and Immunology, Vanderbilt University School of Medicine, Nashville, Tennessee

² Center for Translational Immunology and Infectious Disease, Vanderbilt University Medical Center

³ Vanderbilt Vaccine Center, Vanderbilt University Medical Center, Nashville, Tennessee

⁴ Department of Medicine, Division of Infectious Diseases, Vanderbilt University Medical Center, Nashville, Tennessee

⁵ VA Tennessee Valley Healthcare System, Nashville, Tennessee

⁶ Institute for Immunology and Infectious Diseases, Murdoch University, WA, Australia

⁷ Division of Clinical Pharmacology, Department of Medicine, Vanderbilt University Medical Center, Nashville, Tennessee

⁸ Department of Molecular Physiology and Biophysics, Vanderbilt University School of Medicine, Nashville, Tennessee

*Corresponding Author:

Arion J. Kennedy
Room 702 Light Hall,
Nashville, TN, 37232-0615
Phone: 615-322-5177
Fax: 615-322-8973
Email: arion.kennedy@vanderbilt.edu

Key Words: Obesity, Adipose Tissue, Liver, Clonality, CD8+ T cells

Running Title: Obesity and CD8+ T cell Clonality

ABSTRACT

Adipose tissue (AT) CD4⁺ and CD8⁺ T cells contribute to obesity-associated insulin resistance. Prior studies identified conserved T cell receptor (TCR) chain families in obese AT, but the presence and clonal expansion of specific TCR sequences in obesity has not been assessed. We characterized AT and liver CD8⁺ and CD4⁺ TCR repertoires of mice fed low fat (LFD) and high fat diets (HFD) using deep sequencing of the TCR β chain to quantify clonal expansion, gene usage, and CDR3 sequence. In AT CD8⁺ T cells, HFD reduced TCR diversity, increased the prevalence of public TCR clonotypes, and selected for TCR CDR3 regions enriched in positively-charged and less polar amino acids. While TCR repertoire alone could distinguish between LFD-fed and HFD-fed mice, these properties of the CDR3 region of AT CD8⁺ T cells from HFD-fed mice led us to examine the role of negatively-charged and nonpolar isolevuglandin (isoLG) adduct-containing antigen presenting cells within AT. IsoLG-adducted protein species were significantly higher in AT macrophages of HFD-fed mice; isoLGs were elevated in M2-polarized macrophages, promoting CD8⁺ T cell activation. Our findings demonstrate that clonal TCR expansion favoring positively charged CDR3s accompanies HFD-induced obesity, which may be an antigen-driven response to isoLG accumulation in macrophages.

INTRODUCTION

The stromal vascular fraction of adipose tissue (AT) contains immune cells that contribute to the paracrine signaling milieu that modulates local inflammation and adipocyte function (1). This has been posited to be the primary mechanism by which inflamed AT induces insulin resistance (IR), as inflammatory cytokines are known to interfere with insulin signaling. AT macrophages (ATMs) are thought to serve as the primary cell type responsible for inflammation-induced IR, with AT T cells serving as modulators of ATM activation. However, additional evidence suggests that adaptive immune responses, mediated by both B cells (2, 3) and T cells (4–7), also contribute directly to adverse changes in adipocyte metabolic fitness in obesity.

Regulatory T cells (Tregs) are reduced in obese AT compared to lean AT (6), are protective against AT inflammation and IR, and possess a distinctive gene repertoire (6). Experimental models using adoptive transfer of CD4⁺ T cells into lymphocyte-free Rag1^{-/-} mice reversed weight gain and IR; and depletion of CD8⁺ T cells in AT reduced ATM density and improved insulin sensitivity. These findings suggest that immunotherapy could represent a novel approach to treatment of metabolic disease (4, 8). While the etiology of T cell expansion is unclear at present, *in vitro* studies have found that obese fat independently activates CD8⁺ T cells and induces proliferation, while lean fat has little effect (4).

Spectratyping analyses of AT CD8⁺ T cells in the setting of obesity have also described a narrowed repertoire of T cell receptor (TCR) V α and V β chain families as compared to

cells in lean tissue, suggesting that these CD8⁺ T cells may undergo oligoclonal expansion in AT (4, 9). An important limitation of spectratyping is that it cannot detect individual TCRs, does not provide CDR3 sequences, and only describes deviations from the normally Gaussian distribution of amino acid or nucleotide length. Spectratyping was also used to demonstrate that pro-inflammatory CD4⁺ T_H1 cells with a biased TCR V α repertoire expand in AT, but CD4⁺ T_H17 T cells do not (7). Furthermore, progressive reductions in CD4⁺FoxP3⁺ anti-inflammatory T cells with increasing obesity were detected (7). While spectratyping in these studies allowed the authors to suspect clonal expansion, it did not allow them to quantify TCR repertoire diversity, detect specific clones, examine CDR3 sequences and properties, or examine clonal overlap. Similarly, while analysis of CDR3 α sequences from 98 single AT Treg cells showed that AT Tregs have a unique V gene repertoire (6), the diversity observed and its relation to the native repertoire were less clear as the transgenic mice in this study only carried a single V α gene, were designed to produce a distinctly narrowed TCR repertoire, and have a lower-than-normal thymic output (10).

As prior studies demonstrated that obese mice have increased AT T cell density and a shift towards a pro-inflammatory phenotype, we hypothesized that high fat feeding would induce an increase in AT CD4⁺ and CD8⁺ T cells in conjunction with the clonal expansion of specific TCR clonotypes. We performed high-throughput TCR DNA sequencing of the AT and livers of mice fed either high fat diet (HFD) or low fat diet (LFD). The TCR repertoires of mice on HFD are markedly enriched for public clonotypes in the CD8 and CD4 TCR repertoires of the AT. This overlap in TCRs

between HFD samples was able to distinguish between lean and obese mice, suggesting both selection for more public clonotypes and for autoreactive T cells. We find that the CD8⁺ TCR repertoire of mice on HFD is more clonal and characterized by more charged and less polar complementarity-determining region 3s (CDR3s). These HFD-induced features of the T cell response led us to examine possible sources of neoantigens within AT, specifically the immunogenic and well-characterized isolevuglandin (isoLG) protein adducts, which are the sole lipid neoantigen species that induce a T cell response in hypertension (11). We detected an increase in immunogenic isoLGs, a family of negatively-charged protein adducts generated from reactive γ -ketoaldehydes, in CD206-expressing macrophages isolated from AT of HFD-fed mice. Moreover, isoLGs were elevated in M2-polarized macrophages *in vitro* and co-cultures of these macrophages with T cells promoted CD8⁺ T cell activation. These observations demonstrate that dietary modifications impact the adaptive immune response in AT in a systemic fashion and provide novel insights into potential mechanisms by which HFD diet and obesity may lead to pathogenic T cell responses directed towards modified self-peptides.

RESEARCH DESIGN AND METHODS

Mice and diets. Male C57BL/6J mice were purchased from Jackson Laboratory. Studies were divided into three cohorts; the first cohort was used for AT T cell studies and TCR repertoire analysis, the second was used for isoLGs, and the third was used for measuring isoLGs in ATM subsets and co-culture studies. At 8 weeks of age, mice were placed on 10% LFD for 9 weeks. Subsequently, mice were randomized into either the LFD or HFD dietary groups. Both diets were purchased from Research Diets (New Brunswick, NJ; HFD: D12492, LFD: D12450B). Mice were fed *ad libitum* and given free access to water. All animal procedures were performed with approval from the Institutional Animal Care and Usage Committee of Vanderbilt University.

Glucose tolerance testing. Mice were fasted for 5 hours and basal blood glucose levels were measured (0 minutes) before intraperitoneal administration of 1.5 g dextrose per kg lean body mass. Blood glucose was assessed at 15, 30, 45, 60, 90, and 150 minutes after injection.

AT SVF Isolation, liver NPC isolation, and FACS analysis. AT SVF Isolation: The stromal vascular fraction (SVF) was isolated from epididymal fat pads via collagenase digestion and differential centrifugation as previously described (12). Liver nonparenchymal cell isolation: Liver was excised and minced in 1 mg/ml collagenase in PBS. Minced liver was incubated on shaker at 37°C for 30 min. The cell suspension was filtered and spun at 800×g for 10 min at 4°C. The cell pellet was suspended in 33% Percoll. The Percoll gradient was centrifuged at 800×g for 30 min at room temperature.

Red blood cells were lysed using ACK buffer. Cells were centrifuged at $800\times g$ for 5 min at 4°C . The cells were suspended in FACS buffer and stained for flow cytometry. The following primary fluorophore-conjugated antibodies, along with isotype controls, were used to characterize AT and liver T cell populations: PerCP-Cy5.5-conjugated anti-mouse CD45, APC-conjugated anti-mouse TCR β , Alexa 700-conjugated anti-mouse CD4, and V500-conjugated anti-mouse CD8a (all from eBioscience). DAPI was added immediately prior to analysis to enable discrimination between live and dead cells. FACS was performed on a BD FACSAria III flow cytometer (BD Biosciences) at the Vanderbilt Flow Cytometry Core Shared Resource, and data were analyzed using FlowJo software (Tree Star, Inc.). The gating strategy is shown in Figure S1.

TCR sequencing. Genomic DNA from sorted CD4⁺ and CD8⁺ T cells was isolated using the QIAmp DNA Blood Mini Kit (Qiagen). DNA from AT CD4⁺ and CD8⁺ T cells and liver CD8⁺ T cells was used for bulk TCR β CDR3 region amplification and sequencing using the ImmunoSEQ assay (Adaptive Biotechnologies, Seattle, WA). In this method, bias-controlled V and J gene primers are used to amplify rearranged V(D)J segments for sequencing (13).

IsoLG-adduct quantification. AT macrophages were analyzed by flow cytometry using the following antibodies: PerCP-Cy5.5-conjugated anti-mouse CD64, PE-Cy7-conjugated anti-mouse CD86, Alexa Fluor 700-conjugated anti-mouse CD11c, PE-conjugated anti-mouse CD206, APC-conjugated anti-mouse F4/80, and PECF594-conjugated anti-mouse CD45 (Becton Dickinson). We used intracellular staining with the

single-chain antibody D-11 to detect isoLG protein adducts. The D-11 ScFv antibody was labeled with Alexa Fluor 488 using the APEXTM Alexa Fluor 488 Antibody Labeling kit (Invitrogen). Cells labeled with surface antibodies were fixed and permeabilized for intracellular detection of isoLGs using the FIX & PERM cell permeabilization kit (Invitrogen). Dead cells were excluded from analysis using a LIVE/DEAD® Fixable Dead Cell Stain Kit (Invitrogen). For each experiment, we gated on single live cells and used fluorescence-minus-one (FMO) controls for each fluorophore to establish the gates. Data were analyzed using FlowJo. The gating strategy is shown in Figure S2A.

Bone Marrow-Derived Macrophage (BMDM) polarization and T cell co-culture.

Bone marrow-derived macrophages (BMDM) isolated from C57BL/6J mice were obtained as described by Trouplin *et al* (14). On day 6, fully BMDMs were split and plated into 24 well plates at a density of 700,000 cells per well in L929-conditioned media. Cells were allowed to adhere overnight after which cells were polarized as follows: M1 polarization, BMDMs were stimulated for 24h with IFN- γ (100 ng/mL; R&D Systems) and LPS (10 ng/mL; Sigma); M2 polarization, BMDMs were treated for 96h with IL4 (10 ng/mL; R&D Systems) and IL13 (10 ng/mL; R&D Systems); metabolic polarization (MMe), BMDMs were treated for 24h with 30 mM glucose, 10 nM insulin, and 0.4 mM palmitic acid as described in (15); tert-butyl hydroperoxide (TBHP) treatment, BMDMs were treated with 1 mM TBHP for 30 min, after which the TBHP media was replaced with fresh media. T cells were isolated from spleens of LFD and HFD mice using APC magnetic beads (Miltenyi) to isolate TCR β -APC labelled cells. Polarized BMDMs were co-cultured with isolated pan-T cells from LFD and HFD mice at

a ratio of 1:2. BMDMs and T cells were collected. Immunostaining for flow cytometry was performed using the following antibodies; *Macrophage panel*: PE-conjugated anti-mouse CD45, APC-conjugated anti-mouse F4/80, and intracellular staining with the single-chain antibody D-11 to detect isoLG protein adducts. *Activated T cell panel*: PerCP-Cy5.5-conjugated anti-mouse CD45, FITC-conjugated anti-mouse CD4, PE-CF594-conjugated anti-mouse CD69, and PE-Cy7-conjugated anti-mouse CD8 (BD Bioscience) and DAPI. The gating strategy for BMDMs is shown in Figure S3 and activated T cells in Figure S4.

Computation. Data Import and Pre-processing: All TCR sequences, including non-productive sequences, from ImmunoSEQ were processed and imported using VDJTools as previously described (16). Amino acid sequences were analyzed as the amino acid sequence of a TCR determines its structural properties. Repertoire similarity: VDJTools was used to calculate a pairwise distance matrix between samples, using the geometric mean overlap $F_{ij} = \sqrt{f_{ij}f_{ji}}$ such that $f_{ij} = \sum_{k=1}^N \phi_{ik}$ sums to the frequencies of TCRs shared between two samples present in the first, as the distance metric. This matrix was used to perform complete linkage hierarchical clustering via the *hclust* function in base R (version 3.4.0). Permutation testing was performed to confirm significant factors in clustering. Each sample was downsampled in density-dependent fashion to 10,000 clonal sequences to confirm significant factors in clustering and to confirm significant structure. Mice with less than 1,000 clonotypes detected in any sample were excluded from analysis. Repertoire Overlap: VDJTools' JoinSamples routine was used to detect clonotypes overlapping between samples with shared amino

acid sequences. Clonal Homeostasis: The frequency of each clonotype within each sample was calculated using VDJTools. The clonal space, defined by the sum of frequencies, occupied by the top 1-3, 4-10, 11-20, 21-50, 51-100, and bottom 101-n clonotypes was calculated per sample as described previously (17). These clonal bins were log-transformed and tested for difference in the ratio of their geometric means between LFD and HFD. The CD4 and CD8 clonal bins were then condensed per mouse and used as input for hierarchical clustering. Average linkage was used as the clustering method, and absolute correlation was used as the distance metric. For visualization, the geometric means for each set of samples was calculated per clonal bin and normalized to range from 0-1. t-SNE: Clonal homeostatic proportions were fed into the t-SNE algorithm with principal component analysis (PCA) prior to projection. Perplexity was set at 2, theta at 10^{-5} , learning rate at 1, and perplexity was exaggerated for the first 50 iterations in order to restrain the t-SNE algorithm in size-dependent fashion. 5,000 iterations were allowed. Calculations were performed using the Rtsne package (18). Principal component analysis: Clonal homeostatic proportions were centered and scaled prior to projection. Calculations were performed using the *prcomp* function in base R. P-value validated clustering: Clonal homeostatic proportions were clustered using complete linkage for clustering and absolute correlation for distance. Calculations were performed using the pvclust package (19). Multidimensional scaling: The pairwise distance matrix using geometric mean overlap was used as input for non-metric multidimensional scaling using VDJTools (16) and the *isoMDS* function from the MASS package (20). Repertoire publicity analysis: Public clonotypes were defined as clonotypes being shared between at least 3 mice in order to account for sampling depth.

All public clonotypes were retrieved using VDJTools (16), and the frequency within each mouse was converted to a binary value representing present (1) or absent (0). For each public clonotype, each dietary group was then assigned a binary value representing whether it was greater than the other dietary group (1), lesser (0), or equally prevalent (0). These values were then used to construct a 2×2 contingency table representing the proportion of public TCRs for each dietary group, in similar fashion to analysis of concentration and association (21, 22). Sequence logo plots: Seq2Logo was used to generate three types of sequence logo plots. The median TCR β length was calculated and these sequences were used to generate logo plots utilizing Shannon entropy (the probability of an amino acid appearing), the Kullback-Leibler divergence (probability with enrichment and depletion), and the probability-weighted Kullback-Leibler divergence (probability of each amino acid multiplied by its weight). Where indicated, Hobohm's first algorithm (nearest-neighbor selection clustering) was used to bin TCRs with similar sequences using a threshold of 20% to account for the diversity and divergence of the TCR β chain. A weighted prior correction of 200 pseudocounts based on the BLOSUM-62 matrix was used to correct for amino acids detected at very low levels as previously described (23).

Where appropriate, each mouse's TCR repertoire was also downsampled in density-dependent fashion to 10,000 clonal sequences in order to draw comparisons between samples and to cross-validate the multidimensional structure and similarity of data.

Statistics. Significance was set *a priori* at $P < 0.05$. The following levels of significance are reported: $P \leq 0.05$ (*), $P \leq 0.01$ (**), $P \leq 0.001$ (***), and $P \leq 0.0001$ (****). *Weight and clonality:* Repeated-measures ANOVA with Bonferroni multiple comparisons testing was used to assess changes between diet groups using GraphPad Prism (version 6.05; GraphPad Software, La Jolla, CA) and R (version 3.4.0, RStudio version 1.0.143). *Glucose tolerance testing:* Two-way ANOVA with *post-hoc* Bonferroni-Šídák multiple comparisons testing was used to assess differences between dietary groups at each time point. *Clonal homeostasis:* The Mann-Whitney U test was used to assess differences in the geometric mean ratios of clonal homeostasis bins using GraphPad Prism. *Factor analysis in clustering:* Significant factors in hierarchical clustering were assessed using permutation testing in VDJTools for repertoire similarity. *Cluster analysis in clonal homeostasis:* Cluster significance for clonal homeostatic signatures was assessed using multistep-multiscale bootstrap resampling in the *pvclust* R package (19). *CDR3 amino acid and nucleotide profiling:* CDR3 properties were calculated per sample and per dietary group using VDJTools (16). The Mann-Whitney U and Wilcoxon signed-rank tests were used to assess differences in CDR3 properties using GraphPad Prism and R. P values were corrected using the Benjamini-Hochberg FDR correction. *Repertoire publicity:* We tested the 2×2 contingency table computed as described above using Pearson's χ^2 . The P-value for this test was calculating using Monte Carlo simulation with 1000 bootstraps in R. P values were adjusted using the Bonferroni correction to control the family-wise error rate.

RESULTS

High fat feeding reduces CD8⁺ T cell diversity in AT

A HFD increased body weight (Figure S5A), AT mass (Figure S5B), and liver mass (Figure S5C). While fasting blood glucose was similar among diet groups (Figure S5D), plasma insulin was significantly higher in the HFD mice (Figure S5E) and HFD mice had impaired glucose tolerance (Figure S5F). Next, we compared the T cell density (cells/gram tissue) in AT and liver. Similar to previous studies (4), the density of AT CD8⁺ T cells was elevated by 3-fold in HFD-fed mice compared to LFD-fed controls (Figure 1A). In contrast, AT CD4⁺ T cells and liver CD8⁺ T cells populations were not significantly different between groups (Figure 1B–C).

TCR β chain amplification and deep sequencing of AT CD8⁺ and CD4⁺ T cells as well as liver CD8⁺ T cells yielded three repertoires of V(D)J gene TCR sequences per mouse. These TCR sequences were used to calculate overall repertoire clonality as measured by Shannon entropy using the Adaptive immunoSEQ Analyzer. AT CD8⁺ T cells from HFD-fed mice had a higher clonality score, indicating less diversity, compared to LFD-fed mice (Figure 1D). Although there was somewhat increased clonality in AT CD4⁺ T cells (Figure 1E) and liver CD8⁺ T cells (Figure 1F), this difference was not significant; as we did not detect differences in the liver CD4⁺ populations, we did not sequence these T cells.

T cell clonal distributions differ between mice on HFD or LFD

Our observation of the marked clonality in the CD8⁺ T cells from AT of mice on HFD led us to ask whether diet-induced obesity (DIO) affected the relative contributions of the major and minor clonotypes within a given TCR repertoire. We first examined this clonal homeostatic space within each mouse using the Mann-Whitney U test after downsampling to account for sampling depth. The top clonotypes of mice on HFD occupied significantly higher proportions of clonal space ($P < 0.001$, Figure 2A), while the bottom clonotypes occupied significantly less clonal space ($P < 0.001$) in CD8⁺ T cells from AT and liver. The proportions of these TCRs from the AT and liver also distinguish between lean and obese mice using t-SNE (Figure 2B), PCA (Figure 2C), and hierarchical clustering ($P < 0.05$; Figure 2D). These multidimensional analyses demonstrate that HFD distorts the size of the largest and smallest clonotypes of the repertoire, an observation that traditional measures of clonality such as Shannon entropy do not capture.

Shared clonotypes and gene usage distinguish between TCR repertoires from mice fed LFD or HFD

Hierarchical clustering on repertoire similarity of TCR clonotypes sharing the same amino acid sequence was able to successfully distinguish between both AT CD8⁺ TCR ($P < 0.05$) and AT CD4⁺ TCR repertoires of LFD and HFD mice ($P < 0.001$; Figure 3A). The impact of dietary group on repertoire similarity held true when pooling TCR repertoires from AT and liver and from both CD8⁺ and CD4⁺ T cells ($P = 0.01$; Figure 3B). Expansion of both major and minor clonotypes led to synchronous changes in CD8⁺ T cells between AT and liver repertoires within each mouse (Figure 3C,

Supplementary Table) in a diet-dependent fashion ($P < 0.05$). Each mouse's AT and liver repertoires were most similar to each other, demonstrating the reproducibility of repertoire changes that are tissue-specific.

Our observation of the dissimilarity of the TCR repertoires between dietary groups led us to examine whether $V\beta$ gene usage differed between AT of mice on LFD and HFD. The AT $CD8^+$ T cell repertoires of each dietary group demonstrated differential usage of several $V\beta$ genes (Figure 4A). Neither LFD or HFD impacted $J\beta$ gene usage in the AT (Figure 4B). Similar to other groups, we also observed differential $V\beta$ gene usage between $CD4^+$ and $CD8^+$ T cells (24, 25), which also distinguished between $CD4^+$ and $CD8^+$ TCR repertoires (Figure S6). $CD4^+$ TCRs expressed a decrease in charge and increase in polarity compared to $CD8^+$ TCRs ($P < 0.05$, Figure S7A). They also had characteristically shorter N-D gene-N regions ($P < 0.05$, Figure S7B).

HFD increases the prevalence of public T cell clonotypes

The observation that diet strongly influenced TCR repertoire similarity led us to ask whether HFD-fed mice were more likely to share clonotypes than LFD-fed mice. To test this hypothesis, we utilized a specialized Monte Carlo-validated χ^2 test (Figure S8). This test proved to be robust to both P-value permutation and probability-proportionate-to-size downsampling, in addition to extremely conservative P-value correction. HFD mice were more likely to have public clonotypes shared between at least 3 mice in their $CD8^+$ ($P < 0.001$) and $CD4^+$ AT T cell repertoires ($P = 0.01$). This difference was not observed in the liver $CD8^+$ TCR repertoire.

Regardless of dietary condition and tissue type, we identified 15,419 TCRs shared between any two samples, 9034 TCRs shared between any two CD8⁺ liver samples, 1126 TCRs shared between any two CD4⁺ AT samples, and 826 TCRs shared between any two CD8⁺ AT samples (see Supplementary Information). We also detected previously reported clonotypes that have been associated with obesity and IR in mouse models in both LFD-fed and HFD-fed mice (Table 1).

HFD alters physicochemical properties of the TCR repertoire

In addition to being more clonal, the TCR repertoire of mice on HFD demonstrated marked physicochemical differences from mice on LFD. To assess these differences, we systematically compared the CDR3 of every TCR detected in LFD mice and HFD mice, and CD4⁺ to CD8⁺ TCRs. Obesity resulted in an elevation in charge ($P = 0.01$; Figure 5A) and a decrease in polarity in CD8⁺ TCRs from AT ($P < 0.05$; Figure 5B). These repertoire-level changes do not appear to originate from germline selection, and instead derive from the junctional regions of the CDR3, where TCR diversity is generated at the nucleotide level (Figure 5C, 5D).

To more closely examine the differences in charge and polarity, we utilized sequence entropy measurements to detect enriched and depleted amino acids in the CDR3s of CD8⁺. Weighted Shannon entropy (Figure 6A) and Kullback-Leibler divergence (Figure 6B) demonstrate these changes are due to an enrichment of arginine and depletion of negatively charged amino acids, with other positively charged amino acids selected for

at positions 8, 9, and 11. Unweighted Shannon entropy (Figure 6C) and Kullback-Leibler divergence (Figure 6D), where each TCR is given equal weight, reveal that both lysine and histidine contribute strongly to the increase in charge that we observe.

HFD leads to isoLG accumulation in ATMs

The physicochemical alterations in the CD8⁺ TCR repertoires of HFD-fed mice led us to consider how the CDR3 of the TCR β chain could interact with the local biochemical environment of AT. Because we observed an increased charge and decreased polarity, we chose to examine the isolevuglandin (isoLG) content of antigen-presenting cells within AT, as these highly reactive γ -ketoaldehydes carry both negatively charged phospholipid content and non-polar lipid content (Figure 7A). IsoLGs have been shown to rapidly adduct to lysines on self-proteins, forming isoLG-protein adducts that are processed and presented as neoantigens, and induce an autoimmune-like state in hypertension (11). We isolated total leukocytes from AT and performed flow cytometry to identify isoLG protein adducts in ATMs (Figure 7A). As previously reported from other research groups (26, 27), HFD increased total ATM density and ATM subsets CD11c⁺ (M1-like ATMs), CD206⁺ (M2-like ATMs) and double positive populations (Figure S2B, S2C). After HFD, ATMs showed increased isoLG-adduct formation (Figure 7B) and expression of the co-stimulatory molecule B7 ligand, CD86 (Figure 7C). Regardless of ATM polarization state, HFD led to significant elevations of isoLGs in the number of cells per gram of AT of CD11c⁺, CD206⁺ and CD11c⁺CD206⁺ ATMs compared to LFD (Figure 7D, 7E, 7F). However, HFD only increased the percentage of isoLG⁺ cells in CD206⁺ ATMs (Figure 7E).

Because HFD led to elevations in isoLGs in ATMs, we sought to determine whether isoLGs in macrophages induce T cell activation. As a control and to verify that isoLG-containing macrophages activate T cells, we treated BMDMs with 1 mM tert-butyl hydroperoxide (TBHP), which induces oxidative stress. Treatment with TBHP led to elevations in isoLGs in BMDMs (Figure 8A & B) and as previously reported (11). Using an *in vitro* co-culture system, we polarized BMDMs to M1, M2, and obesogenic metabolically activated macrophages (MMe) to represent the various subsets present in AT during HFD. Surprisingly, isoLG levels were only elevated in M2-polarized macrophages compared to M0 ($P < 0.05$), were lower in M1 macrophages ($P < 0.001$) and were not different in MMe macrophages compared to M0 (Figure 8A & 8B). TBHP-treated and polarized BMDMs were subsequently cultured with pan-T cells isolated from spleens of LFD and HFD mice. As expected, co-culture with TBHP-treated macrophages led to elevations of total CD8⁺ T cells (Figure 8C) and more specifically in activated cells as indicated by expression of the early activation marker, CD69 (Figure 8D). Furthermore, only the isoLG-containing M2 macrophages promoted an increase in CD8⁺ T cells and their activation (Figure 8C & D) and this was only when co-cultured with CD8⁺ T cells from the obese HFD-fed mice. Together these findings demonstrate that ATMs express isoLGs under obese conditions and isoLG-containing M2 macrophages are capable of driving CD8⁺ T cell activation *in vitro*.

DISCUSSION

We demonstrate that HFD-fed mice have a higher AT CD8⁺ T cell density and TCR clonality. CD8⁺ cells from AT of HFD-fed mice also have a distinctive TCR repertoire that differs in both charge and polarity within the CDR3 region compared to LFD-fed mice. These changes are not observed within the CD4⁺ TCR repertoire, which utilizes different V segment genes than CD8⁺ T cells regardless of diet (Figure 4A). The repertoires of mice on HFD are also more public than mice on LFD, which has previously been reported in autoimmune pathologies but uncommonly in anti-pathogen responses (reviewed in 28). Furthermore, we provide evidence that these repertoire properties may emerge in part as a response to an increase in immunogenic isoLG-adducts present in the ATMs of mice on a HFD. Here we have directly identified and quantitated specific clonally expanded TCRs within the CD8⁺ and CD4⁺ T cell populations that appear to arise in response to diet-induced obesity. We also demonstrate that the AT TCR repertoire alone can distinguish between LFD and HFD mice. To that end, we note that HFD induces repertoire-level changes previously described in studies of autoimmunity and enriches for amino acid sequences biased towards a positive charge. In fact, Glanville *et al.* have recently described a strong inverse correlation between CDR3 charge and epitope charge in TCRs of both humans and mice (29). Lastly, we document elevated numbers of isoLG⁺ macrophages in the AT of HFD-fed mice, and that M2 macrophages containing isoLG-adducted protein enhance T cell survival and activation. These data suggest a coordinated mechanism of inflammation within AT, wherein T cells infiltrate tissue in response to neoantigen presented on ATMs.

To date, other studies have described the infiltration of a possibly clonally expanded T cell population within AT (4, 7, 10, 30). In mice, Yang *et al.* observed shifts in the clonality of both the AT CD4⁺ and CD8⁺ TCR repertoires in obese vs lean mice using PCR-based spectratyping, where clonal expansion was detected as a deviation from the normally Gaussian frequency distribution of CDR3 length (10). While spectratyping has been advantageous in the detection of unusual T cell clones in lymphoma, it does not provide the specificity or direct measurement of clonal expansion and cannot distinguish between expanded clones with different amino acid sequences and similar V and J gene usage. Consequently, spectratyping also cannot detect clones with identical amino acid sequences and different V and J gene usage, as we observe in the CD8⁺ and CD4⁺ TCR repertoires of mice on both LFD and HFD (Supplementary Information). In contrast, deep sequencing of the TCR repertoire makes it possible to distinguish between the TCR repertoires of mice on LFD or HFD (Figure 3) and to assess intricate biochemical details of the TCR at the repertoire level (Figure 4-6). Similar observations have been made with regards to HFD-induced T cell infiltration in pancreatic islets (31–35), skeletal muscle (36), and liver (37). We observed similar levels of macrophage and CD8⁺ T cell infiltration as reported in prior studies, and further identified several highly oligoclonal CD8⁺ T cell populations induced by HFD. As previously reported by Nishimura *et al.* (4), we observed no difference in CD4⁺ T cell infiltration into AT and extend this observation to include no significant difference in CD4⁺ T cell clonality (P = 0.18). While we do not observe enrichment of V β gene families 7 and 10b as in (4), we do observe slight enrichment of V β families 17, 18, 21, 22, 25, 27, 28, and 29 (Figure

4A). We observe a pronounced increase in the clonality of CD8⁺ T cells in AT of HFD-fed mice and note that future studies should specifically examine the extent to which this is induced by diet alone or entirely dependent on obesity. Future dietary studies would also benefit from analysis of age, as at least one study indicates that adipose tissue mass and CD8⁺ T cells—but not CD4⁺ T cells—are elevated independent of diet in aging male and female mice (38).

Highly clonal T cell populations have been described in a broad array of pathologies (39). Our group has recently demonstrated that the TCR repertoire is more clonal in the AT of obese and overweight HIV-infected adults on long-term therapy compared to blood, and the V-J gene family pairings appeared to differ between the tissue compartments (30), suggesting that similar repertoire contraction also occurs in the adipose tissue of humans. Adverse effects of similarly clonal populations have been described in both obesity and diabetes. Highly clonal T cell populations recognizing an HLA-DR4-restricted epitope of insulin have been documented in type 1 diabetic patients (40). Obesity in both mice and humans leads to markedly lower naïve T cell pools and highly clonal T cell populations, further restricting the availability of diverse TCRs (41). A recent report by Pham *et al.* indicates that HFD also limits the diversity of the B cell repertoire, which corresponds with IR (2). The presence of a clonally expanded T cell population within tissue can be explained by several immunological processes. One possible scenario is that a T cell population may infiltrate in response to an antigen within the tissue, as documented in AT of humans and macaques during chronic SIV and HIV infection (42). Another is the presence of multiple T cell populations sharing the

same TCR but with drastically different functional roles and properties (43). Alternatively, dominant clones from the blood could enter the tissue in an antigen-blind fashion.

Our findings raise the question of where and how antigen is presented to drive TCR clonal expansion. Several published reports indicate that antigen presentation to CD4⁺ T cells occurs directly in AT. Multiple MHC-II-expressing APC populations in AT can present to CD4⁺ T cells, including B cells (3), dendritic cells (44), macrophages (45), and even adipocytes (46). Mice with global deficiency of MHC-II demonstrate protection from AT inflammation and systemic IR when placed on HFD (45). A portion of the reduced inflammation in AT was due to attenuation of CD11c⁺ macrophages and CD4⁺ T cell accumulation (45). There are also adipokines that can directly activate these APCs, including leptin, adiponectin, and retinol binding protein 4 (46–48). Thus, AT has all the prerequisite components to activate CD4⁺ T cells. However, our studies show clonality in the CD8⁺ T cell population, begging the question of their activation signals. MHC-I is expressed on all cell types and could allow for presentation of neoantigens or modified proteins. Our data suggest an enrichment of arginine and positively charged amino acids in the TCRs of CD8⁺ T cells that are clonally expanded in HFD-fed mice. This positive charge led us to consider that protein modifications leading to a negative charge might serve as neoantigens in AT. Indeed, our data suggest that macrophages from AT display increased levels of isoLG-adducts (Figure 7). Similar alterations in charge and amino acid content have been reported in the context of renal disease (11, 49). Insulin-reactive TCRs have recently been reported to be enriched for arginine and

for non-polar amino acids at position 7 (50), which we also observe. We identified TCRs previously associated with obesity and IR in mice (Table 1), two of which were significantly enriched in HFD TCR repertoires. One clonotype that was highly prevalent in AT is known to be insulin-reactive, and another is known to be enriched in the pancreas of diabetic mice. In contrast, two previously reported diabetogenic clonotypes were detected at elevated levels in LFD-fed mice alone (Table 1). This demonstrates that changes to the TCR repertoire extend to multiple tissues in the context of obesity and IR, and that insulin reactivity alone may not explain clonal expansion within AT. While we did not observe significant changes in the TCR repertoire of CD4⁺ T cells of the adipose tissue, future studies could also examine the TCR repertoire of CD4⁺ T cells within the liver, where fat also accumulates during diet-induced obesity.

Our findings suggest isoLGs may act as neoantigens responsible for AT TCR clonal expansion. Generation of these reactive lipid aldehydes is primarily dependent on oxidative stress and they are detected at elevated levels in other autoimmune processes, including multiple sclerosis, glaucoma, allergic inflammation, and cancer (reviewed in 53). Previous studies examined the role of various lipid adducts on the immunogenicity of APC and found that only proteins adducted to isolevuglandins (isoLGs) induced APC immunogenicity (11). A number of published reports demonstrate oxidative stress levels are elevated in AT of obese mice and humans (54, 55). In pulmonary injury, impaired NADPH oxidase reduces production of isoLG-adducted proteins, while impairment of the Nrf2-antioxidant response element signaling pathway increases isoLG-modified protein levels (56). Furthermore, inhibition of NADPH oxidase

reduces obesity-induced AT ROS production, inflammation, and insulin resistance (54, 55). Thus, obesity-induced oxidative stress in ATMs may account for the elevation in isoLGs.

While our results suggest that M2-like ATMs induce or enhance clonal expansion of AT-infiltrating T cells through the presentation of immunogenic isoLG-adducted peptides, the extent to which ATM-generated isoLGs induce clonal expansion in T cells remains to be explored. We also note that T cells derived from splenocytes in the liver may not precisely reflect those found in adipose tissue, and that a culture model able to effectively enrich such lymphocytes from the adipose tissue would be a valuable contribution to the field. Our results also suggest several new directions for further investigation. The antigen specificity of clonally expanded T cells within AT remains to be determined, and single-cell TCR sequencing can connect surface phenotype information from flow cytometry with transcriptomics and paired TCR $\alpha\beta$ sequences (51). Though we did not identify any clonotypes that were universally shared at high (>1%) frequencies between or within diet groups, we did observe several TCRs that were shared within the top 100 clonotypes of each dietary group (Table 1 and available upon request), particularly with respect to HFD-fed mice. This suggests that the antigens or neoantigens presented in obesity may not be the same from mouse to mouse. These TCRs may be specific for one or more antigens, though we have previously shown that T_H1 CD4⁺ cells, CD8⁺ T cells, and memory cells accumulate in the AT of weight cycled mice, suggesting secondary immune responses with repeat exposure to HFD (52), and our *in vitro* experiments suggest that isoLG-containing macrophages augment T cell

activation and survival in tissue resident immune populations that are expanded in obesity (Figure 8). In summary, we have demonstrated that T cells infiltrating AT of obese mice are clonally expanded, that the TCR repertoires of lean and obese mice are distinct in their sequences and biochemical properties, that immunogenic isoLGs are elevated in ATMs of obese mice, and that T cells of obese mice accumulate and activate in response to isoLG-containing M2 macrophages. Our observations also suggest that therapy targeting the CD8⁺ T cell population and antigens thereof could potentially abrogate inflammation and other consequences of adaptive immune activation in obesity.

AUTHOR CONTRIBUTIONS

Conceptualization, A.J.K., A.H.H., W.J.M., J.R.K., S.A.M., M.A.P.; Methodology, A.J.K., A.H.H., W.J.M., J.R.K., S.A.M., M.A.P.; Software, W.J.M.; Validation, W.J.M., A.J.K., A.K., M.A.C., M.K.K., J.R.K., A.H.H.; Formal Analysis, W.J.M., A.J.K., J.R.K.; Investigation, W.J.M., A.J.K., M.A.P., M.A.C., A.K., M.K.K.; Resources, A.H.H., J.R.K., S.A.M.; Data Curation, W.J.M., A.J.K., J.R.K., A.H.H.; Writing – Original Draft, W.J.M., A.J.K., J.R.K., A.H.H.; Writing, Review & Editing – all authors; Visualization, W.J.M., A.J.K.; Supervision, A.J.K., J.R.K., S.A.M., A.H.H.; Project Administration, A.J.K., J.R.K., S.A.M., A.H.H.; Funding Acquisition, A.J.K., J.R.K., S.A.M., A.H.H.

ACKNOWLEDGMENTS

WJM was supported by funding from T32 award HL069765 and is supported by R01 award DK112262. AJK is supported by K01 award HL121010. This work was supported by a Merit Award from the Veterans Affairs (5I01BX002195) to AHH who is also supported by an Innovation Award from the American Diabetes Association (1-17-IBS-140). JRK was supported by K23 award AI100700-06 and is supported by R01 award DK112262. MAC is supported by funding from T32 award DK007563. Flow cytometry was performed in the VMC Flow Cytometry Shared Resource, supported by the Vanderbilt Ingram Cancer Center (CA68485) and the Vanderbilt Digestive Disease Research Center (DDRC; DK058404), from which AHH received a scholarship. TCR sequencing was performed in the Vanderbilt Technologies for Advanced Genomics core laboratory. This study was supported by Tennessee Center for AIDS Research grant P30 AI110527; the funders had no role in study design, data collection and analysis, decision to publish, or preparation of the manuscript. These data were presented in part at the Inaugural Immunometabolism and Chronic Disease Conference in Coral Coast, Fiji, May 13-16 2017, the 18th International Winter Eicosanoid Conference in Baltimore, MD, March 11-14, 2018, and the 7th Annual Southeastern Immunology Symposium, Birmingham, AL, June 16-17, 2018. Dr. Arion Kennedy and Mr. Wyatt McDonnell are the guarantors of this work and, as such, had full access to all the data in the study and take responsibility for the integrity of the data and the accuracy of the data analysis.

COMPETING FINANCIAL INTERESTS

The authors have declared no conflicts of interest.

MATERIALS AND CORRESPONDENCE

Correspondence and requests for materials should be addressed to AJK.

DATA AVAILABILITY

The data that support the findings of this study are available from the corresponding author upon request.

FIGURE LEGENDS

Figure 1. *HFD leads to increased T cell number and clonality.*

HFD increases T cell number and repertoire clonality within AT. **(A)** AT CD8⁺ number was increased in HFD mice (two-tailed *t*-test), while **(B)** CD4⁺ T cells were not significantly increased. **(C)** There was no difference in the number of liver CD8⁺ T cells ($P > 0.05$). **(D)** The TCR repertoires of AT CD8⁺ T cells of HFD-fed mice are significantly more clonal than those of LFD-fed mice ($P < 0.05$, two-tailed Student's *t*-test). **(E)** AT CD4⁺ clonality did not differ between HFD and LFD ($P = 0.18$, two-tailed Student's *t*-test). **(F)** Liver CD8⁺ T cells of HFD-fed mice are not significantly clonal in comparison to LFD-fed mice ($P = 0.18$, two-tailed Student's *t*-test). Data points represent the clonality of each mouse as calculated using normalized Shannon entropy. Data are presented as mean \pm SEM, $n = 4$ -5 mice/group.

Figure 2. *Clonal homeostatic space differs between dietary groups and is a distinctive signature in multidimensional space.*

HFD alters the frequency within the repertoire occupied by the largest and smallest TCR clonotypes. **(A)** The space within the repertoire occupied by the clonotypes within each clonal bin was calculated for each mouse. The geometric mean for each of these proportions was calculated for each diet group, and the clonal homeostatic proportions occupied were tested using the two-tailed Mann-Whitney U test. The clonal proportions distinguish between dietary conditions using modern machine learning methods measuring several multidimensional distances. **(B)** 2D t-SNE projection of clonal homeostatic proportions from the adipose tissue and liver reveals that lean and obese mice differ in clonal homeostasis as measured in a 2D projection. PCA with centering and scaling was performed prior to t-SNE, and 15 dimensions were retained for embedding with the t-SNE algorithm. **(C)** PCA projection of clonal homeostatic proportions reveals that the repertoire space occupied by both highly and lowly abundant clonotypes distinguishes between lean and obese mice. **(D)** Hierarchical clustering using average linkage and absolute correlation reveals that clonal homeostatic proportions distinguish between lean and obese mice. Values shown at each node demonstrate the confidence that a cluster truly exists as measured using multiscale bootstrap resampling (shown in red on left) and traditional bootstrapping (shown in green on right). Multiscale bootstrap resampling validates that these characteristic differences are not expected to distinguish between lean and obese mice by chance alone.

Figure 3. *Dietary group is predictive of repertoire similarity and synchronously alters the TCR repertoire in AT.*

Geometric mean overlap was used to calculate pairwise distance matrices on the basis of shared clonotypes with identical CDR3 amino acid sequences. Labels on each dendrogram correspond to a specific mouse, tissue type (A = adipose, L = liver) and cell type (4 or 8). **(A)** AT CD4⁺ (left) and CD8⁺ repertoires (right) share more TCRs within diet groups than between diet groups. ($P < 0.0001$ for CD8⁺ and $P < 0.0001$ for CD4⁺, permutation of pairwise distance matrix). This suggests that sets of shared TCRs are enriched and depleted in a diet-dependent fashion. **(B)** Diet significantly impacts repertoire similarity across multiple cell types and within multiple tissues ($P = 0.01$, permutation of pairwise distance matrix). TCRs shared between mice within multiple tissue and T cell types distinguish between lean and obese mice. Diet-dependent repertoire similarity is observed in liver in addition to adipose tissue, while **(C)** CD8⁺ T cell repertoires from liver and AT reflect simultaneous clonal expansion and sharing within each mouse and show that diet significantly impacts repertoire similarity within the CD8⁺ compartment ($P < 0.05$, permutation of pairwise distance matrix).

Figure 4. *CD8⁺ TCR repertoires within AT are genetically distinct by dietary group.*

Z-score normalized heatmaps were built using VDJTools. Labels underneath the heatmaps correspond to individual mice, and rows correspond to a given V β gene. The heatmap is colored on the basis of Z-score and how many standard deviations from the mean a given sample is in its expression of a given V β gene family. **(A)** Obesity leads AT CD8⁺ T cells to use distinct sets of V gene segments. These changes do not appear

to distinguish between CD4⁺ T cells of lean and obese mice, though CD4⁺ T cells appear to use different sets of V β genes than CD8⁺ T cells regardless of dietary condition. **(B)** Obesity does not impact the J segments used within the CD8⁺ TCR repertoires of mice to the same extent that V segments do. This is unsurprising, as there are fewer J β genes than V β genes, and as the J β region frequently accounts for less nucleotide diversity than the V β region.

Figure 5. CD8⁺ TCR repertoires of mice on HFD differ in physicochemical properties in comparison to those of mice on LFD.

Analysis of different segments of the CDR3 reveals differences in amino acid properties between HFD and LFD TCR repertoires. **(A)** AT CD8⁺ T cell repertoires of obese mice are significantly higher in charge ($P = 0.01$, Student's t -test). This elevation in charge is due to amino acids encoded in the junctional regions of the TCR, where diversity is generated. **(B)** The CD8⁺ T cell repertoire within AT is also markedly lower in polarity in obese mice ($P < 0.01$, Student's t -test). Unlike the changes observed in charge, the difference in polarity appears to arise from germline selection. **(C)** Elevations in charge arise from the junctional regions of the TCR, where TCR diversity is generated at the nucleotide level. Repertoires were assessed using 3 scanning bins to account for variance along each region and to identify signal arising from each genetic region of the TCR. **(D)** The increased polarity of AT CD8⁺ TCR repertoires from obese mice appears to be more closely related to changes selected at the germline level, unlike changes in charge.

Figure 6. *CDR3 analysis reveals enrichment for positively charged amino acids and depletion of negatively charged amino acids in the CD8⁺ TCR repertoires of mice on HFD.*

Weighted and unweighted measures of entropy demonstrate selection for positively charged amino acids within the CDR3 of HFD TCR repertoires. The median CDR3 length was 14 amino acids, which we analyzed using several sequence entropy methods. **(A)** Shannon entropy reveals enrichment of arginine and depletion of negatively charged amino acids in the CD8⁺ repertoires of HFD-fed mice. **(B)** P-weighted Kullback-Leibler divergence with Hobohm1 clustering reveals that other positively-charged amino acids are enriched within HFD CD8⁺ TCR repertoires from AT and that negatively charged amino acids are correspondingly depleted. Unweighted analyses using Shannon entropy **(C)** and P-weighted Kullback-Leibler divergence **(D)** show that these amino acid enrichments are due to clonotypes present at higher frequencies, though there is still enrichment for arginine, lysine, and histidine, all of which carry a positive charge at physiological pH. This indicates that obesity-induced changes in charge and polarity at the repertoire level are not only driven by highly expanded clonotypes but also by clonotypes that are present at lower frequencies.

Figure 7. *HFD induces formation of immunogenic isolevuglandins (isoLGs) and expression of B7 ligand CD86 in ATMs.*

Total leukocytes were isolated from AT of mice fed LFD or HFD, and isoLG content was quantified using previously described gating schema. **(A)** Structure of the major isoLG protein adducts. The major intermediates are a pair of pyrrolic epimers whose

covalently bonded nitrogen originates from lysine residues on proteins. Phospholipids attached to isoLGs derive from polyunsaturated acids, arachidonic acids, and phospholipids thereof. **(B)** Flow cytometry representatives and average data showing intracellular staining for isolevuglandin-protein adducts in ATMS using the single-chain antibody D-11 ScFv. **(C)** Flow cytometry representatives and average data showing surface expression of CD86 and isoLGs in ATMs (proportion of ATMs staining CD86⁺isoLG⁺). Flow cytometry representatives and average data showing the number of isoLG⁺ cells per gram of tissue and percent of isoLG⁺ cells per ATM subsets CD11c⁺ **(D)**, CD206⁺ **(E)**, and CD11c⁺CD206⁺ **(F)** ATMs of HFD-fed mice. Data are presented as mean ± SEM, n = 5–10 mice/group.

Figure 8. *M2 polarization increases IsoLGs levels and promotes activation of CD8⁺ T cells.*

BMDMs were polarized to M0, M1, M2, MMe, or treated with TBHP. Following polarization, BMDMs were co-cultured with isolated T cells from the spleen of mice fed a LFD or HFD for 3 days. IsoLG content was quantified in polarized BMDMs by flow cytometry. **(A)** Flow analysis and **(B)** quantification of IsoLG⁺ F4/80⁺ cells (one-way ANOVA). Data are presented as mean ± SEM, n = 3 wells/group. T cells were collected from co-cultures and flow analysis was performed to quantify **(C)** CD8⁺ T cells and **(D)** CD8⁺CD69⁺ T cells (two-way ANOVA). Data are presented as mean ± SEM, n = 5 mice/group. Data are presented as mean ± SEM, n = 5 wells/group.

1 **Table 1.** Detection of previously reported T cell clonotypes associated with pathogenesis in mouse models of obesity and
 2 diabetes. *References:* (1) Thelin, M. A. *et al.* In Vivo Enrichment of Diabetogenic T Cells. *Diabetes* (2017).
 3 doi:10.2337/db16-0946. (2) Candéias, S., Katz, J., Benoist, C., Mathis, D. & Haskins, K. Islet-specific T-cell clones from
 4 nonobese diabetic mice express heterogeneous T-cell receptors. *Proc. Natl. Acad. Sci. U. S. A.* 88, 6167–6170 (1991).
 5 (3) DiLorenzo, T. P. *et al.* Major histocompatibility complex class I-restricted T cells are required for all but the end stages
 6 of diabetes development in nonobese diabetic mice and use a prevalent T cell receptor alpha chain gene rearrangement.
 7 *Proc. Natl. Acad. Sci. U. S. A.* 95, 12538–12543 (1998). (4) Analysis of the Repertoire of Insulin-Reactive CD8+ T cell,
 8 J.A. Pearson. 2014. <https://orca.cf.ac.uk/68395/1/2014PearsonJAPhD.pdf>. (5) Lennon, G. P. *et al.* T cell islet
 9 accumulation in type 1 diabetes is a tightly regulated, cell-autonomous event. *Immunity* 31, 643–653 (2009). (6). Pearson,
 10 J. A. *et al.* Proinsulin Expression Shapes the TCR Repertoire but Fails to Control the Development of Low-Avidity Insulin-
 11 Reactive CD8+ T Cells. *Diabetes* 65, 1679–1689 (2016).
 12

CDR3 AA	Reference	HFD Liver CD8	HFD Adipose CD8	HFD Adipose CD4	LFD Liver CD8	LFD Adipose CD8	LFD Adipose CD4	Annotation	P-value
CASSLGSGNTLYF	(1)	4	1	1	3	0	0	Expanded in pancreas	n.s.
CASSDAGQYEQYF	(1)	1	0	0	2	0	0	Expanded in pancreas	n.s.
CASSDSAETLYF	(1)	3	3	0	1	0	0	Expanded in pancreas	*
CASGDEGYEQYF	(1)	1	0	1	0	0	0	Expanded in pancreas	n.s.
CASGDAREQYF	(1)	2	1	0	3	0	0	Expanded in pancreas & B cell scaffolds	n.s.
CASGSSYEQYF	(1)	2	0	1	2	0	0	Expanded in beta cell scaffolds	n.s.
CASSDAGTTNERLFF	(1)	1	0	1	0	0	0	Expanded in beta cell scaffolds	n.s.
CASGSSYEQYF	(1)	2	0	1	2	0	0	Expanded in beta cell scaffolds	n.s.
CASSLGTGDEQYF	(2)	2	1	1	1	0	1	Diabetogenic clone BDC 4.12	n.s.
CASSGTGGQNTLYF	(3)	0	0	0	3	0	0	Diabetogenic clone AI15.A3, beta cell autoreactive	*
CASSGTGGQNTLY	(3)	0	0	0	3	0	0	Diabetogenic clone AI5.F5, beta cell autoreactive	*
CASSLGGYEQYF	(4)	3	1	3	5	1	2	Pro-insulin reactive	n.s.
CASSRDNTEVF	(4)	3	0	1	2	0	0	Insulin reactive	n.s.
CASSLTGNTGQLY	(4)	2	0	4	1	0	0	Insulin reactive	*
CASSPDNYEQY	(4)	1	1	1	2	0	0	Insulin reactive	n.s.
CASSRHQDTQYF	(5)	1	0	0	2	0	0	Specificity not known	n.s.
CASSLGGYEQY	(6)	3	1	2	5	1	2	Reactive against insulin	n.s.

REFERENCES

1. Kohlgruber AC, LaMarche NM, Lynch L. Adipose tissue at the nexus of systemic and cellular immunometabolism. *Semin. Immunol.* 2016; 28(5):431–440.
2. Pham TD *et al.* High-fat diet induces systemic B-cell repertoire changes associated with insulin resistance. *Mucosal Immunol.* 2017; 10(6):1468. doi:10.1038/mi.2017.25
3. Winer DA *et al.* B cells promote insulin resistance through modulation of T cells and production of pathogenic IgG antibodies. *Nat. Med.* 2011; 17(5):610–617.
4. Nishimura S *et al.* CD8+ effector T cells contribute to macrophage recruitment and adipose tissue inflammation in obesity. *Nat. Med.* 2009; 15(8):914–920.
5. Duffaut C, Galitzky J, Lafontan M, Bouloumié A. Unexpected trafficking of immune cells within the adipose tissue during the onset of obesity. *Biochem. Biophys. Res. Commun.* 2009; 384(4):482–485.
6. Feuerer M *et al.* Lean, but not obese, fat is enriched for a unique population of regulatory T cells that affect metabolic parameters. *Nat. Med.* 2009; 15(8):930–939.
7. Winer S *et al.* Normalization of obesity-associated insulin resistance through immunotherapy. *Nat. Med.* 2009; 15(8):921–929.
8. Stolarczyk E *et al.* Improved insulin sensitivity despite increased visceral adiposity in mice deficient for the immune cell transcription factor T-bet. *Cell Metab.* 2013; 17(4):520–533.
9. Yang H *et al.* Obesity increases the production of proinflammatory mediators from adipose tissue T cells and compromises TCR repertoire diversity: implications for systemic inflammation and insulin resistance. *J. Immunol.* 2010; 185(3):1836–1845.
10. Correia-Neves M, Waltzinger C, Mathis D, Benoist C. The shaping of the T cell repertoire. *Immunity* 2001; 14(1):21–32.
11. Kirabo A *et al.* DC isoketal-modified proteins activate T cells and promote hypertension. *J. Clin. Invest.* 2014; 124(10):4642–4656.
12. Orr JS, Kennedy AJ, Hasty AH. Isolation of Adipose Tissue Immune Cells. *J. Vis. Exp.* [published online ahead of print: May 22, 2013]; (75). doi:10.3791/50707
13. Robins H *et al.* Ultra-sensitive detection of rare T cell clones. *J. Immunol. Methods* 2012; 375(1–2):14–19.
14. Trouplin V *et al.* Bone marrow-derived macrophage production. *J. Vis. Exp.* 2013; (85): 50966. doi: 10.3791/50966.
15. Hill AA *et al.* Activation of NF- κ B drives the enhanced survival of adipose tissue macrophages in an obesogenic environment. *Molecular Metabolism.* 2015; 4(10): 665-677.
16. Shugay M *et al.* VDJtools: Unifying Post-analysis of T Cell Receptor Repertoires. *PLoS Comput. Biol.* 2015; 11(11):e1004503.
17. Nazarov VI *et al.* tcR: an R package for T cell receptor repertoire advanced data analysis. *BMC Bioinformatics* 2015; 16:175.
18. Krijthe JH. Rtsne: T-Distributed Stochastic Neighbor Embedding using a Barnes-Hut Implementation. [Internet]. 2015.
19. Suzuki R, Shimodaira H. Pvcust: an R package for assessing the uncertainty in

- hierarchical clustering. *Bioinforma. Oxf. Engl.* 2006; 22(12):1540–1542.
20. Ripley BD, Venables WN. *Modern applied statistics with S-PLUS*. Springer Science & Business Media; 2013.
 21. Feoli E, Orlóci L. Analysis of concentration and detection of underlying factors in structured tables. *Vegetatio* 1979; 40(1):49–54.
 22. Williams EJ. Use of Scores for the Analysis of Association in Contingency Tables. *Biometrika* 1952; 39(3/4):274.
 23. Thomsen MCF, Nielsen M. Seq2Logo: a method for construction and visualization of amino acid binding motifs and sequence profiles including sequence weighting, pseudo counts and two-sided representation of amino acid enrichment and depletion. *Nucleic Acids Res.* 2012; 40(Web Server issue): W281-287.
 24. Candéias S, Waltzinger C, Benoist C, Mathis D. The V beta 17+ T cell repertoire: skewed J beta usage after thymic selection; dissimilar CDR3s in CD4+ versus CD8+ cells. *J. Exp. Med.* 1991; 174(5):989–1000.
 25. Emerson R *et al.* Estimating the ratio of CD4+ to CD8+ T cells using high-throughput sequence data. *J. Immunol. Methods* 2013; 391(1–2):14–21.
 26. Nawaz A *et al.* CD206+ M2-like macrophages regulate systemic glucose metabolism by inhibiting proliferation of adipocyte progenitors. *Nat. Commun.* 2017; 8(1):286.
 27. Li P *et al.* Functional heterogeneity of CD11c-positive adipose tissue macrophages in diet-induced obese mice. *J. Biol. Chem.* 2010; 285(20):15333–15345. doi: 10.1074/jbc.M110.100263.
 28. Madi A *et al.* T-cell receptor repertoires share a restricted set of public and abundant CDR3 sequences that are associated with self-related immunity. *Genome Res.* 2014; 24(10):1603–1612.
 29. Glanville J *et al.* Identifying specificity groups in the T cell receptor repertoire. *Nature* 2017; 547(7661):94–98.
 30. Koethe JR *et al.* Adipose Tissue is Enriched for Activated and Late-differentiated CD8+ T cells, and Shows Distinct CD8+ Receptor Usage, Compared to Blood in HIV-infected Persons. *JAIDS J. Acquir. Immune Defic. Syndr.* 2018; 77(2):e14-21.
 31. Butcher MJ *et al.* Association of proinflammatory cytokines and islet resident leucocytes with islet dysfunction in type 2 diabetes. *Diabetologia* 2014; 57(3):491–501.
 32. Brooks-Worrell B, Narla R, Palmer JP. Islet autoimmunity in phenotypic type 2 diabetes patients. *Diabetes Obes. Metab.* 2013; 15 Suppl 3:137–140.
 33. Sarikonda G *et al.* CD8 T-cell reactivity to islet antigens is unique to type 1 while CD4 T-cell reactivity exists in both type 1 and type 2 diabetes. *J. Autoimmun.* 2014; 50:77–82.
 34. Lennon GP *et al.* T cell islet accumulation in type 1 diabetes is a tightly regulated, cell-autonomous event. *Immunity* 2009; 31(4):643–653.
 35. Wang J *et al.* In situ recognition of autoantigen as an essential gatekeeper in autoimmune CD8+ T cell inflammation. *Proc. Natl. Acad. Sci. U. S. A.* 2010; 107(20):9317–9322.
 36. Khan IM *et al.* Attenuated adipose tissue and skeletal muscle inflammation in obese mice with combined CD4+ and CD8+ T cell deficiency. *Atherosclerosis* 2014; 233(2):419–428.

37. Wolf MJ *et al.* Metabolic activation of intrahepatic CD8⁺ T cells and NKT cells causes nonalcoholic steatohepatitis and liver cancer via cross-talk with hepatocytes. *Cancer Cell* 2014; 26(4):549–564.
38. Ahnstedt H, *et al.* Sex differences in adipose tissue CD8⁺ T cells and regulatory T cells in middle-aged mice. *Front. Immunol.* 2018; 9:659. doi: 10.3389/fimmu.2018.00659.
39. Miles JJ, Douek DC, Price DA. Bias in the $\alpha\beta$ T-cell repertoire: implications for disease pathogenesis and vaccination. *Immunol. Cell Biol.* 2015; 89(3):375–387.
40. Kent SC *et al.* Expanded T cells from pancreatic lymph nodes of type 1 diabetic subjects recognize an insulin epitope. *Nature* 2005; 435(7039):224–228.
41. Yang H *et al.* Obesity accelerates thymic aging. *Blood* 2009; 114(18):3803–3812.
42. Damouche *et al.* Adipose tissue is a neglected viral reservoir and an inflammatory site during chronic HIV and SIV infection. *PLoS Pathogens.* 2015; 11(9):e1005153. doi: 10.1371/journal.ppat.1005153.
43. Bilate AM *et al.* Tissue-specific emergence of regulatory and intraepithelial T cells from a clonal T cell precursor. *Sci. Immunol.* 2016; 1(2):eaaf7471-eaaf7471.
44. Cho KW *et al.* Adipose Tissue Dendritic Cells Are Independent Contributors to Obesity-Induced Inflammation and Insulin Resistance. *J. Immunol.* 2016; 197(9):3650–3661.
45. Cho KW *et al.* An MHC II-dependent activation loop between adipose tissue macrophages and CD4⁺ T cells controls obesity-induced inflammation. *Cell Rep.* 2014; 9(2):605–617.
46. Mattioli B, Straface E, Quaranta MG, Giordani L, Viora M. Leptin promotes differentiation and survival of human dendritic cells and licenses them for Th1 priming. *J. Immunol.* 2005; 174(11):6820–6828.
47. Jung MY, Kim H-S, Hong H-J, Youn B-S, Kim TS. Adiponectin induces dendritic cell activation via PLC γ /JNK/NF- κ B pathways, leading to Th1 and Th17 polarization. *J. Immunol.* 2012; 188(6):2592–2601.
48. Moraes-Vieira PM *et al.* RBP4 activates antigen-presenting cells, leading to adipose tissue inflammation and systemic insulin resistance. *Cell Metab.* 2014; 19(3):512–526.
49. Wu H, Zhang GY, Knight JF. T cell receptor BV gene usage in interstitial cellular infiltrates in active Heymann nephritis. *Nephrol. Dial. Transplant. Off. Publ. Eur. Dial. Transpl. Assoc. - Eur. Ren. Assoc.* 2001; 16(7):1374–1381.
50. Pearson JA *et al.* Proinsulin Expression Shapes the TCR Repertoire but Fails to Control the Development of Low-Avidity Insulin-Reactive CD8⁺ T Cells. *Diabetes* 2016; 65(6):1679–1689.
51. Schober K, Busch DH. A synergistic combination: using RNAseq to decipher both T-cell receptor sequence and transcriptional profile of individual T cells. *Immunol. Cell Biol.* 2016; 94(6):529–530.
52. Anderson EK, Gutierrez DA, Kennedy A, Hasty AH. Weight cycling increases T-cell accumulation in adipose tissue and impairs systemic glucose tolerance. *Diabetes* 2013; 62(9):3180–3188.
53. Salomon RG, Bi W. Isolevuglandin Adducts in Disease. *Antioxid. Redox Signal.* 2015; 22(18):1703–1718.
54. Den Hartigh LJ *et al.* Adipocyte-Specific Deficiency of NADPH Oxidase 4 Delays

- the Onset of Insulin Resistance and Attenuates Adipose Tissue Inflammation in Obesity. *Arterioscler. Thromb. Vasc. Biol.* 2017; 37(3):466–475.
55. Coats BR *et al.* Metabolically Activated Adipose Tissue Macrophages Perform Detrimental and Beneficial Functions during Diet-Induced Obesity. *Cell Rep.* 2017; 20(13):3149–3161.
 56. Mont S *et al.* Accumulation of isolevuglandin-modified protein in normal and fibrotic lung. *Sci. Rep.* 2016; 6(1). doi:10.1038/srep24919

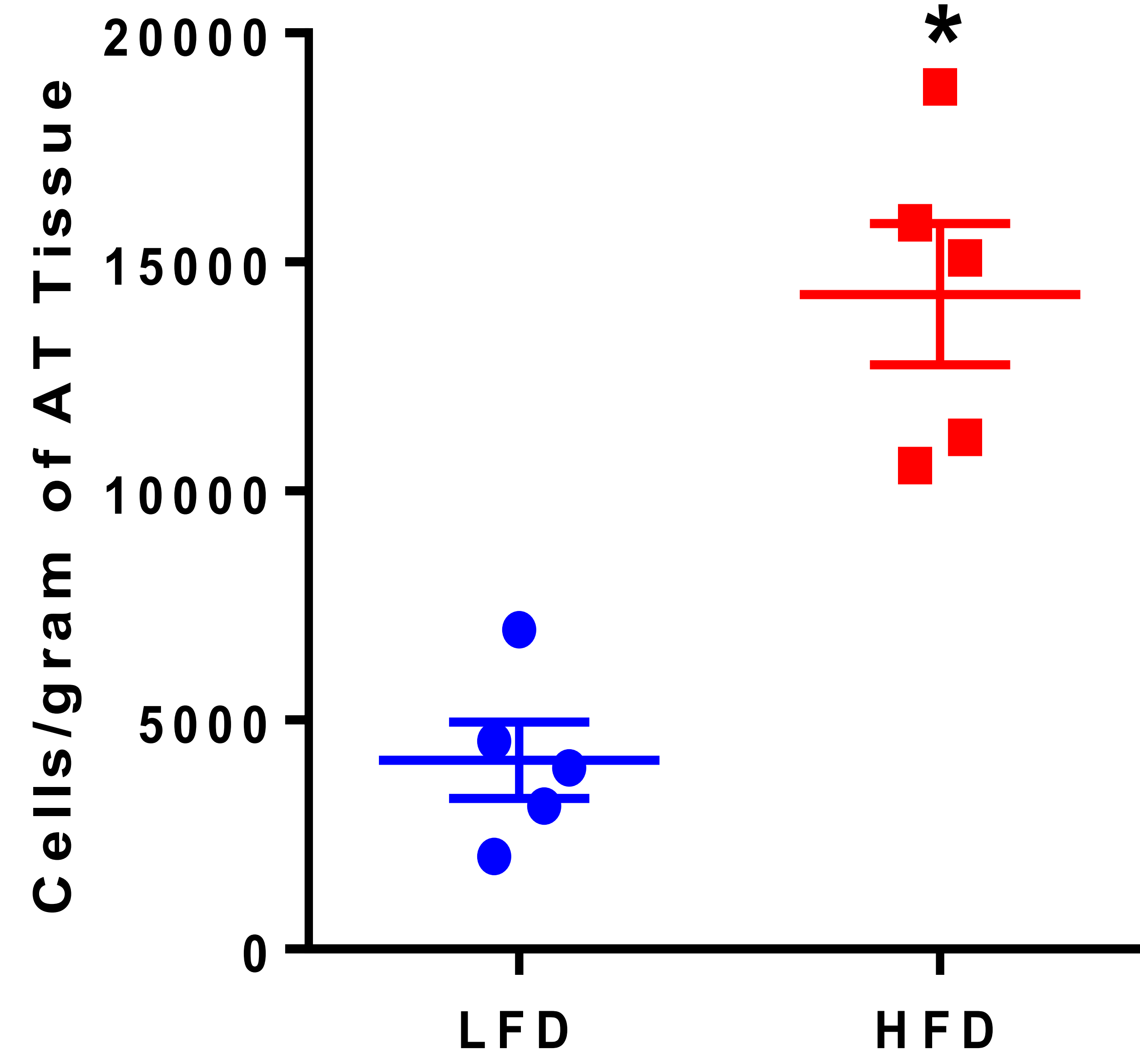
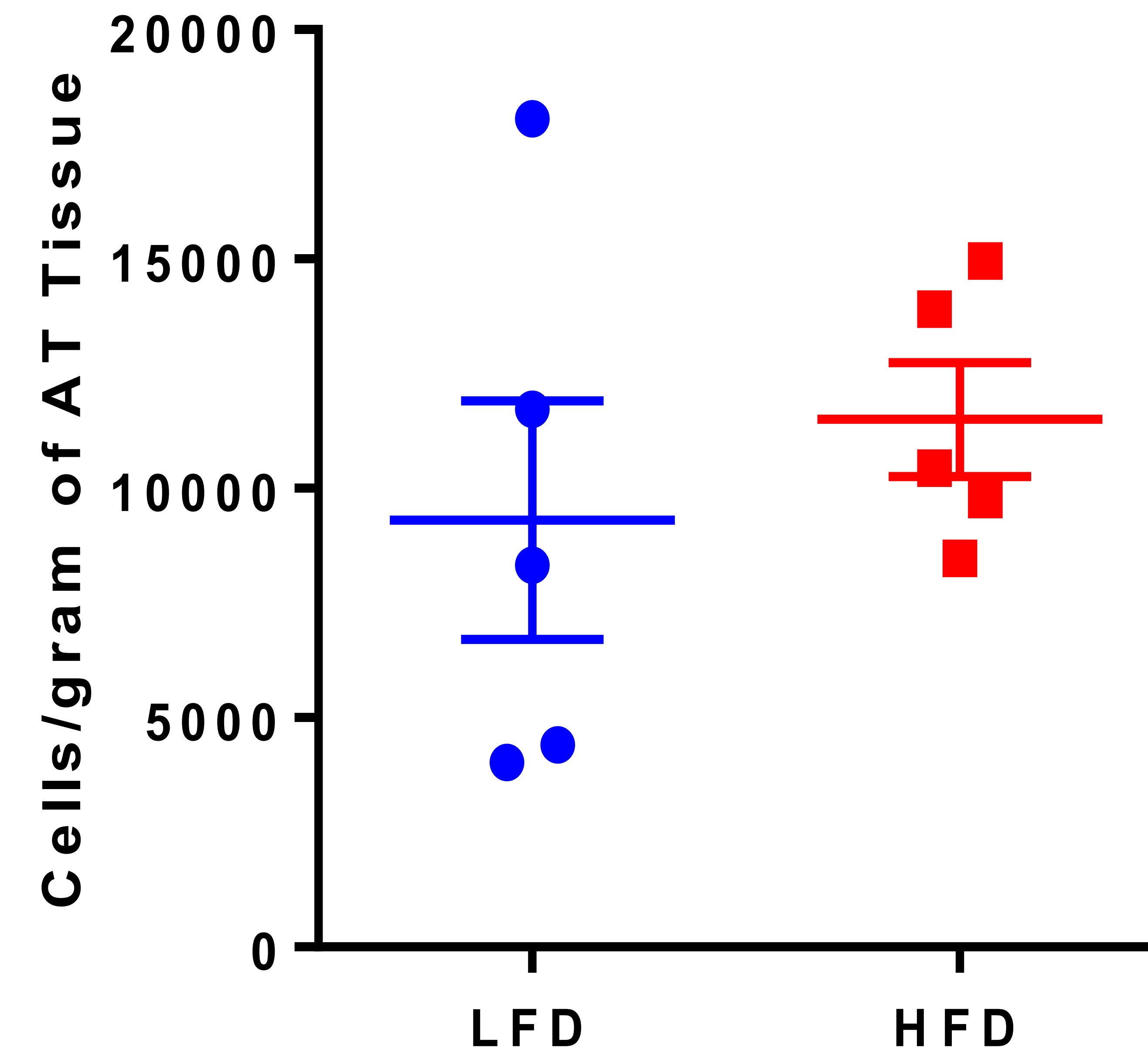
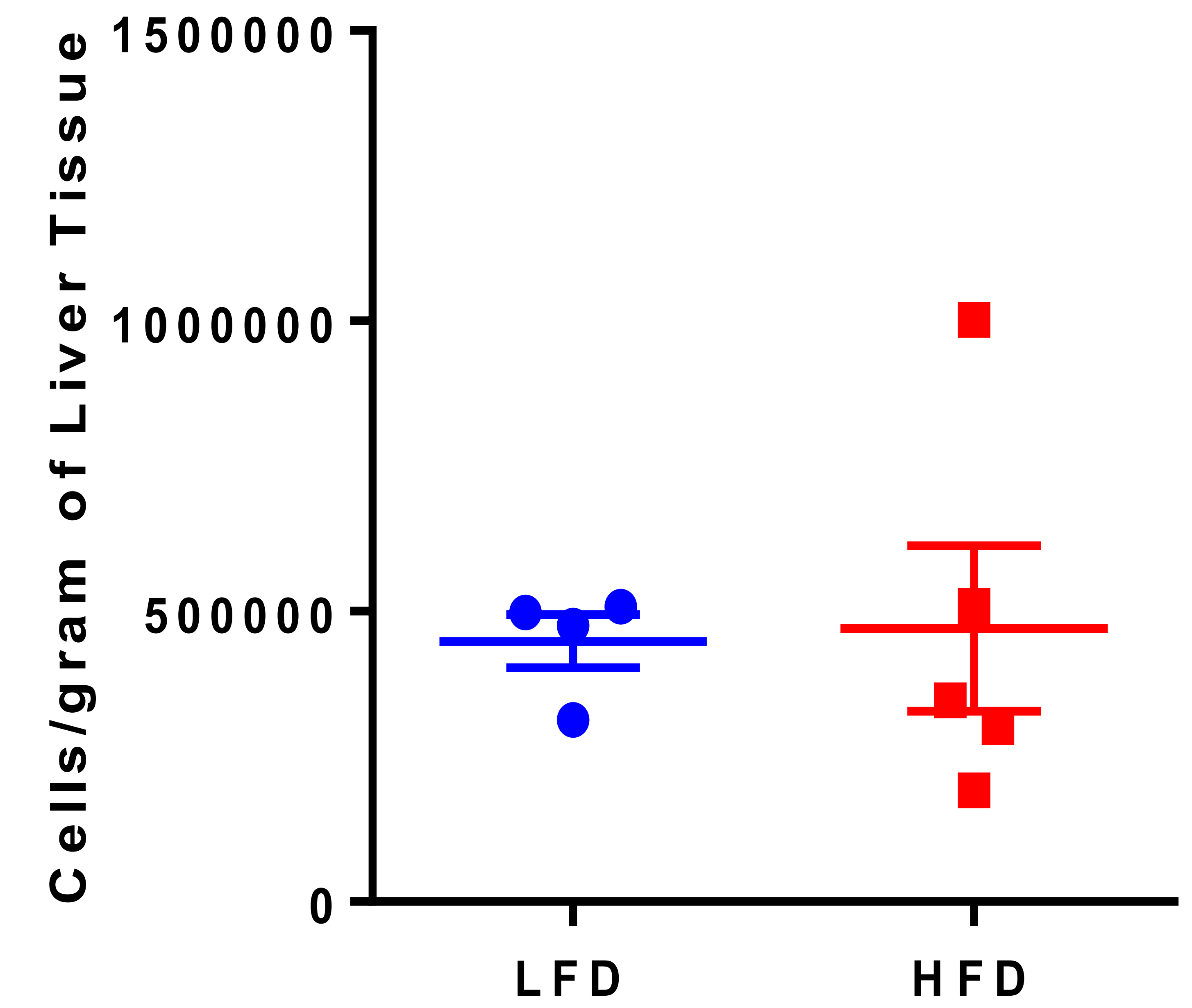
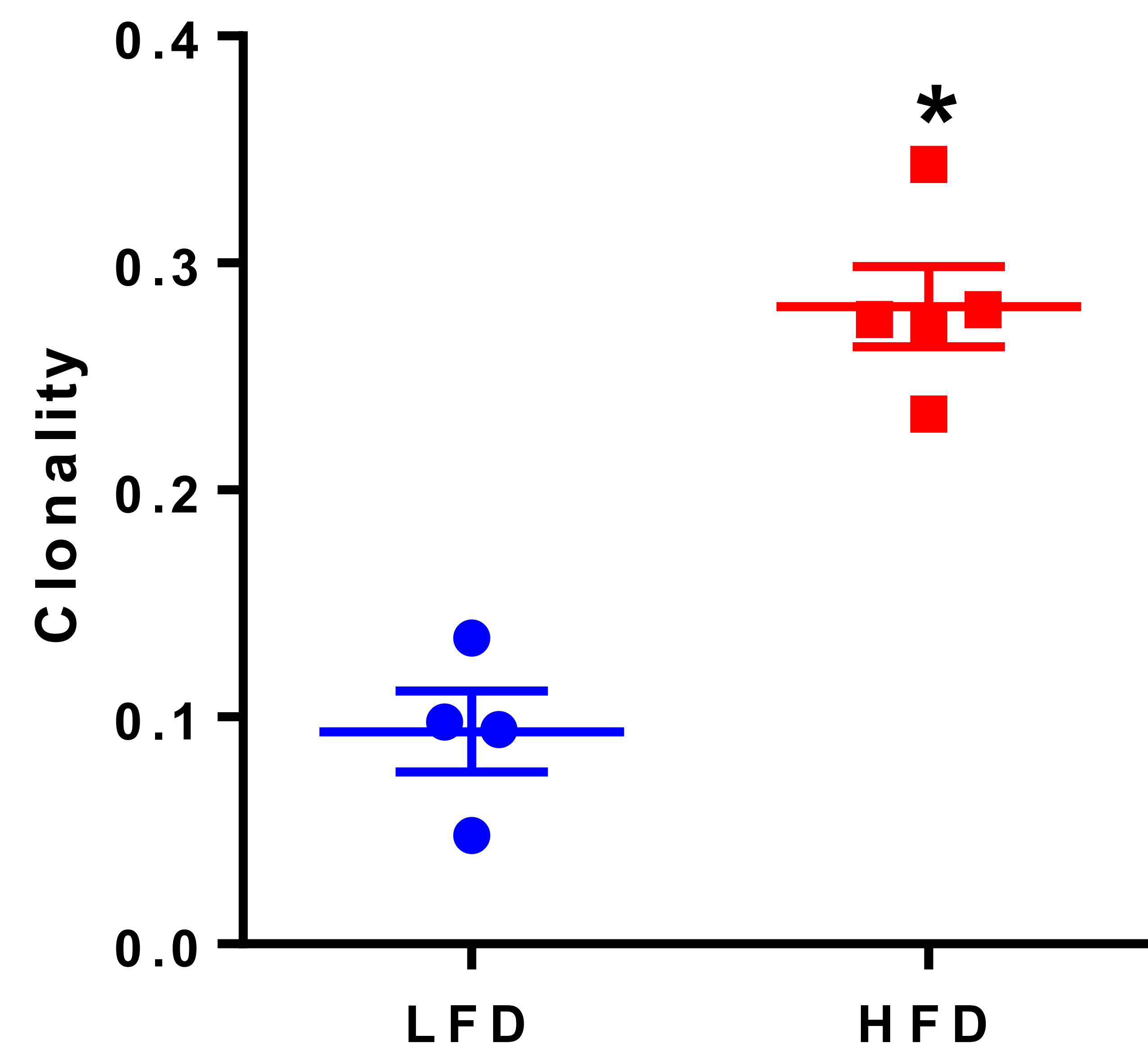
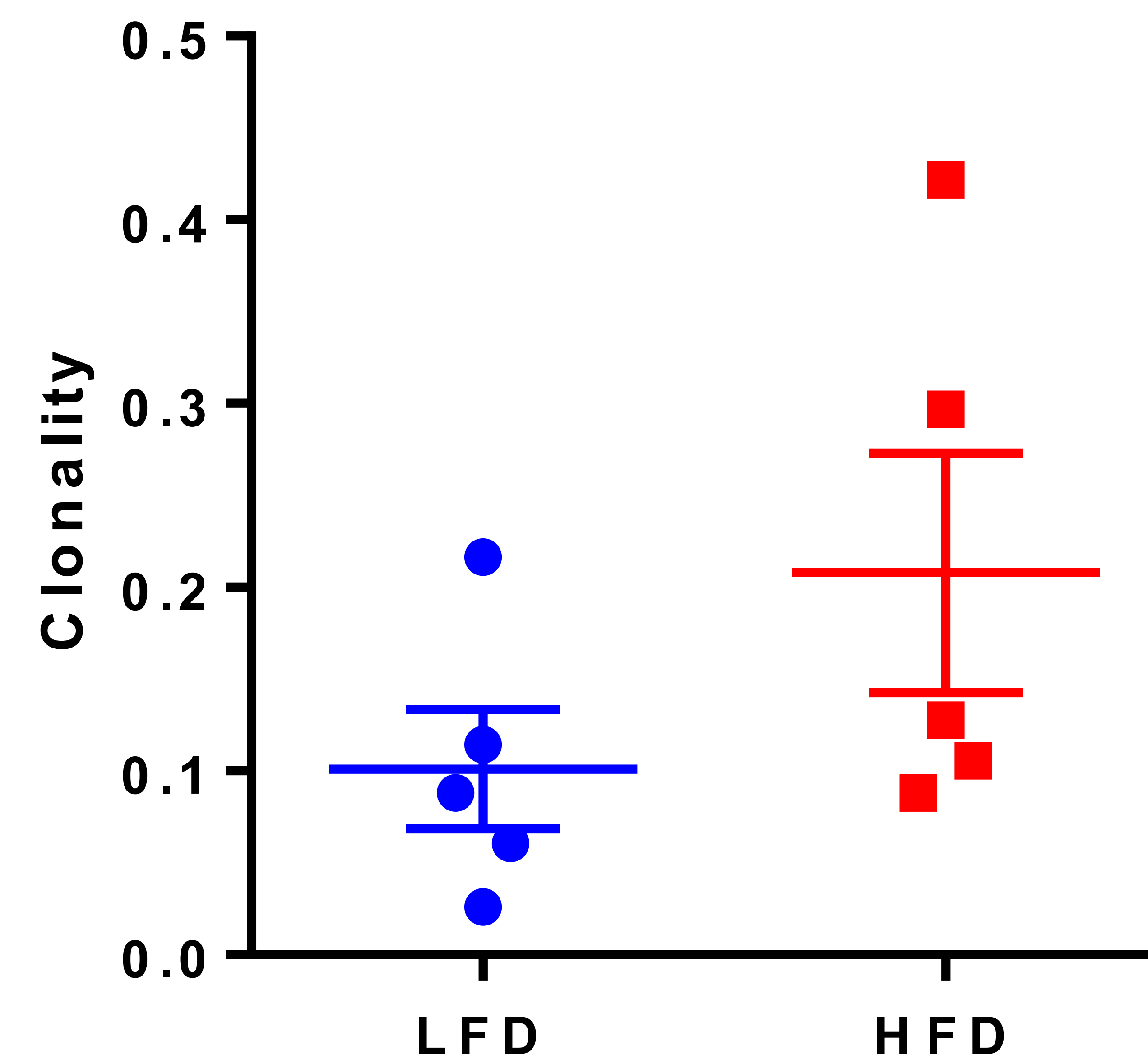
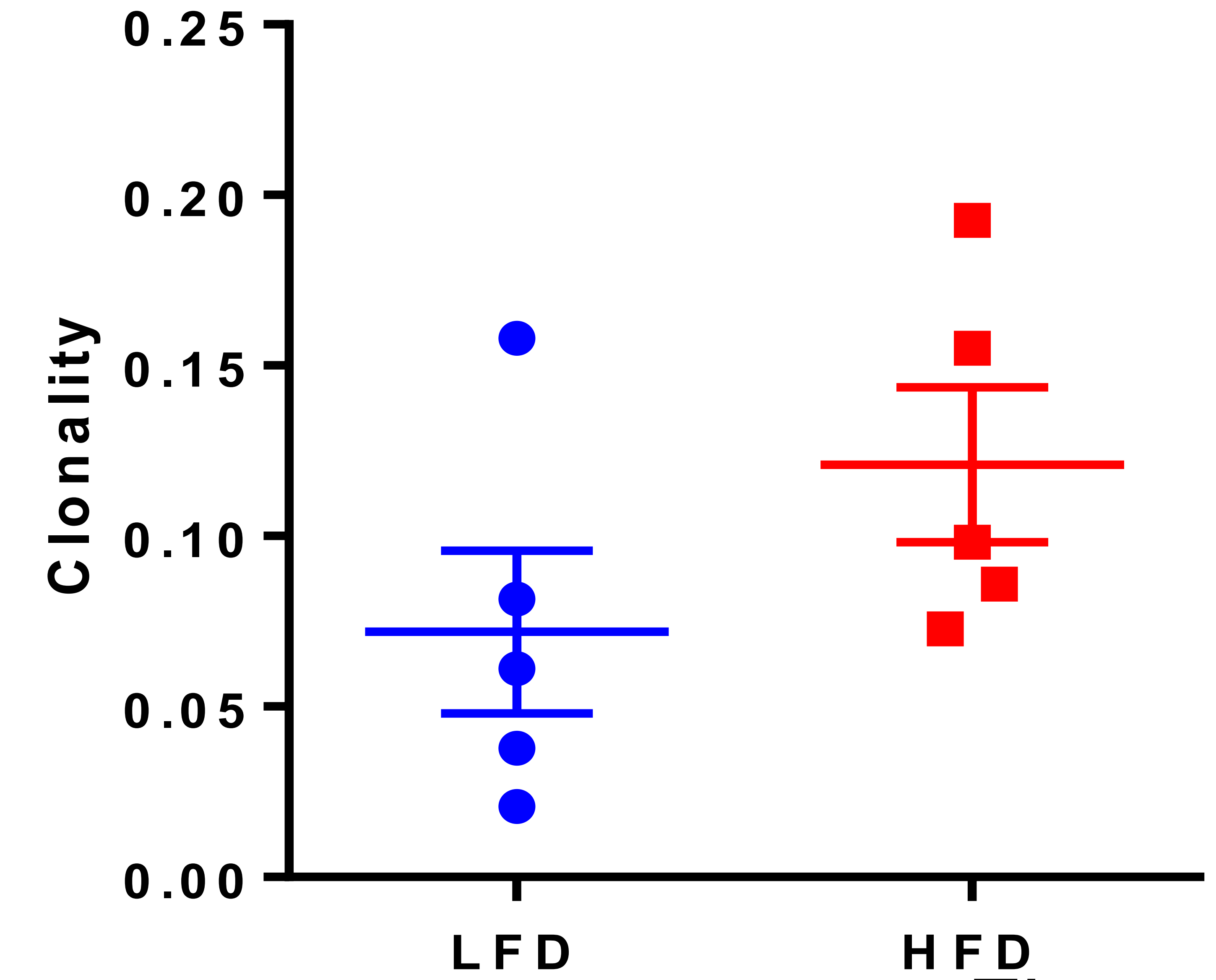
AAT CD8⁺ T cells**B**AT CD4⁺ T cells**C**Liver CD8⁺ T cells**D**AT CD8⁺ T cells**E**AT CD4⁺ T cells**F**Liver CD8⁺ T cells

Figure 1

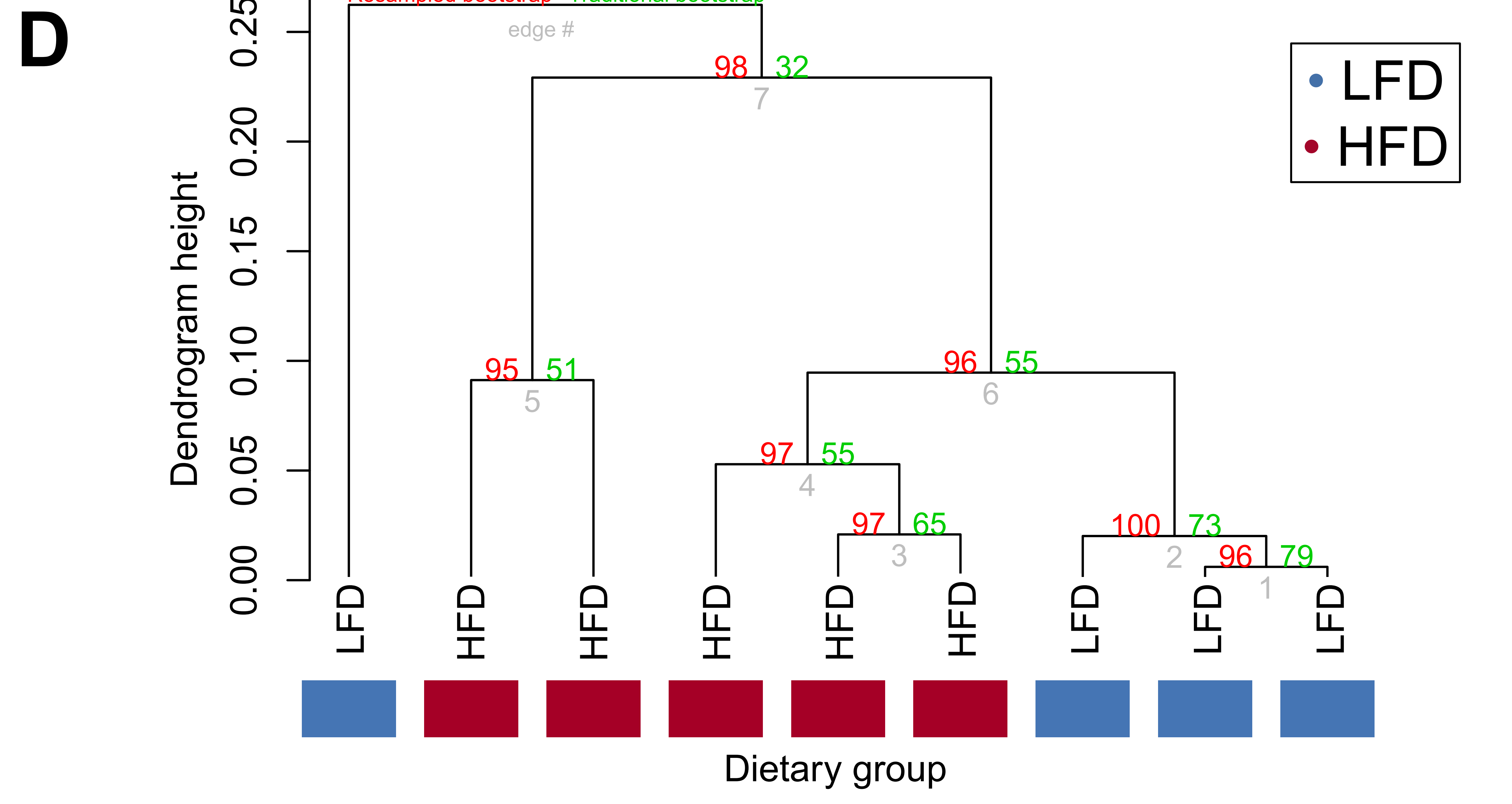
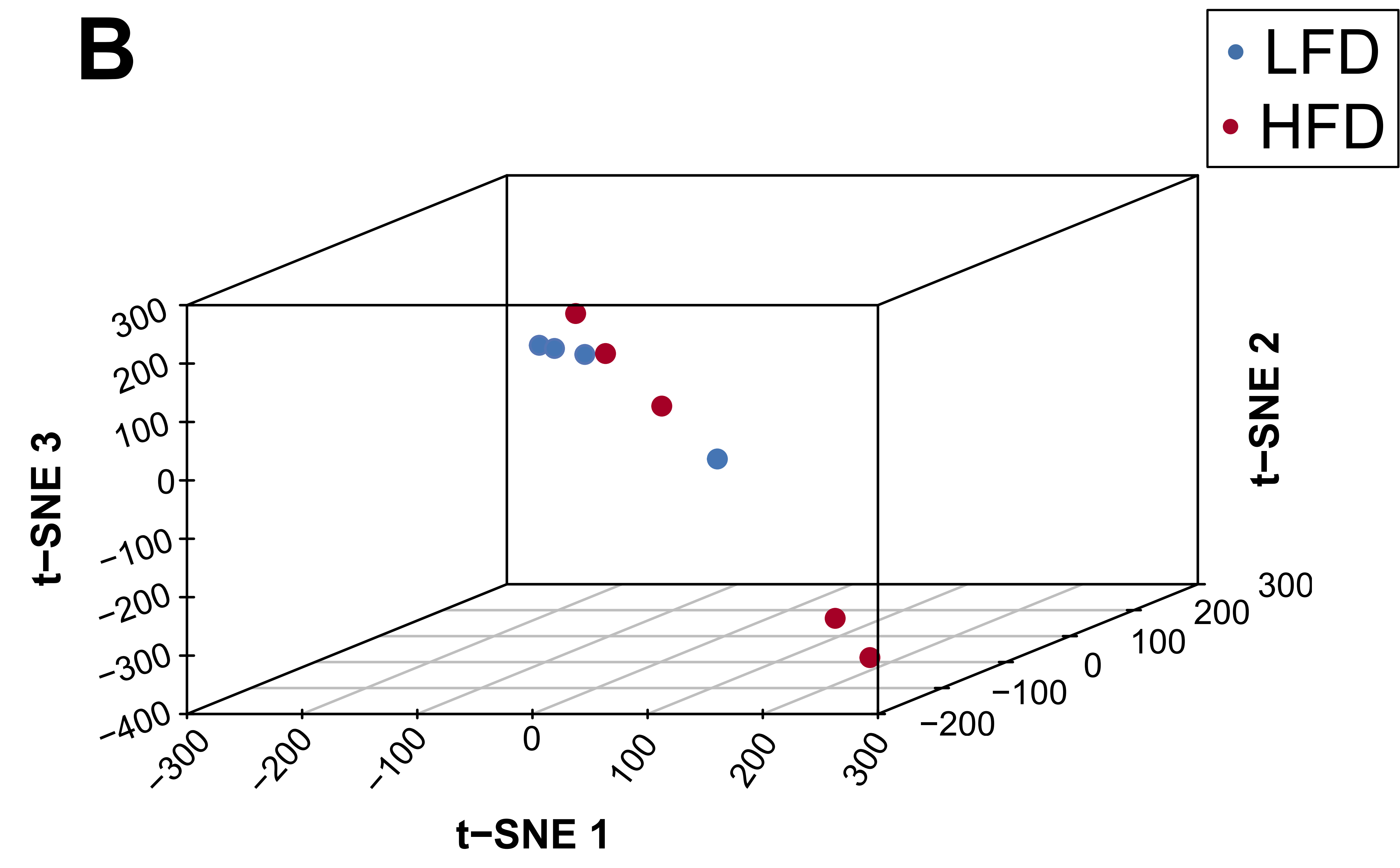
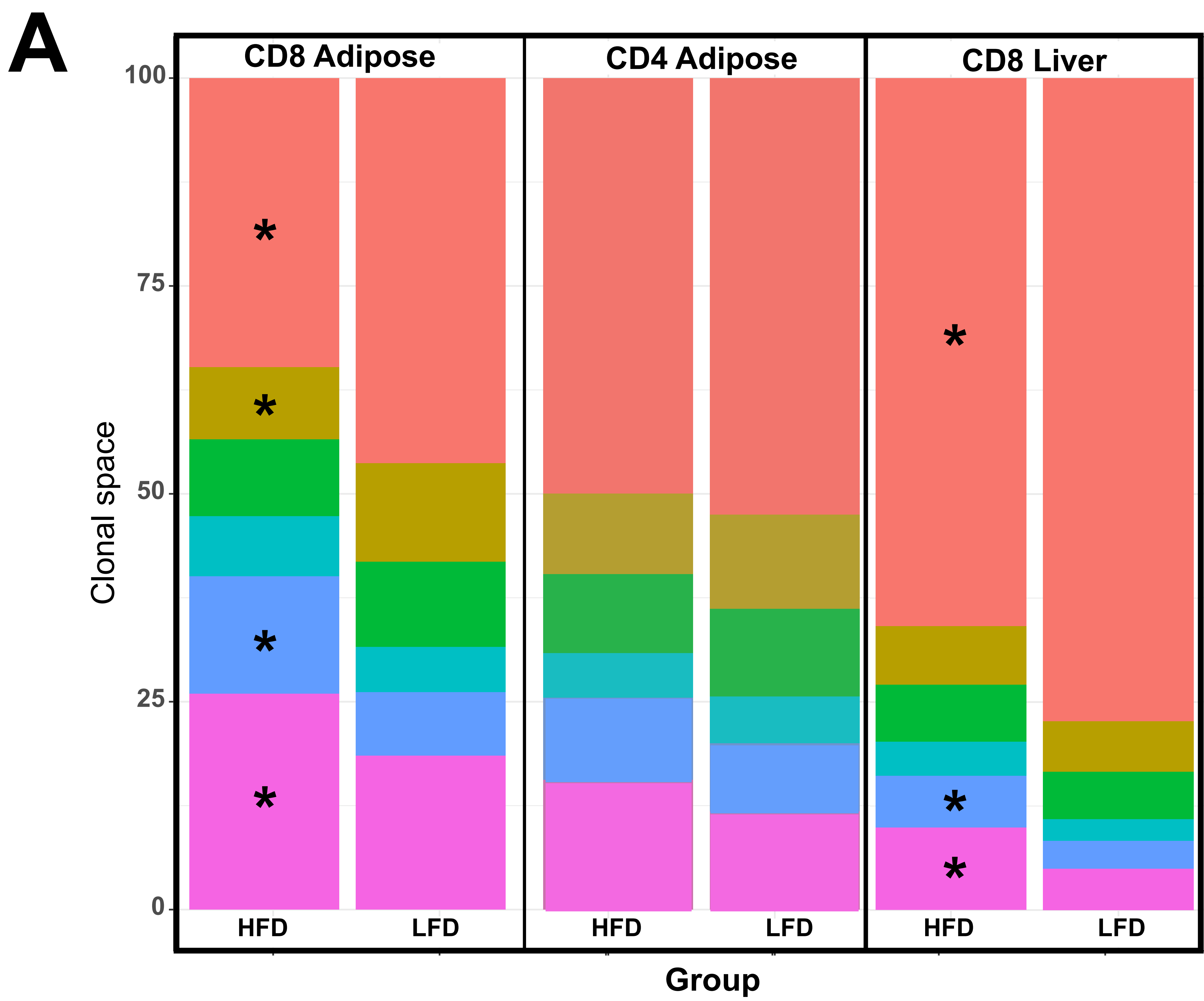
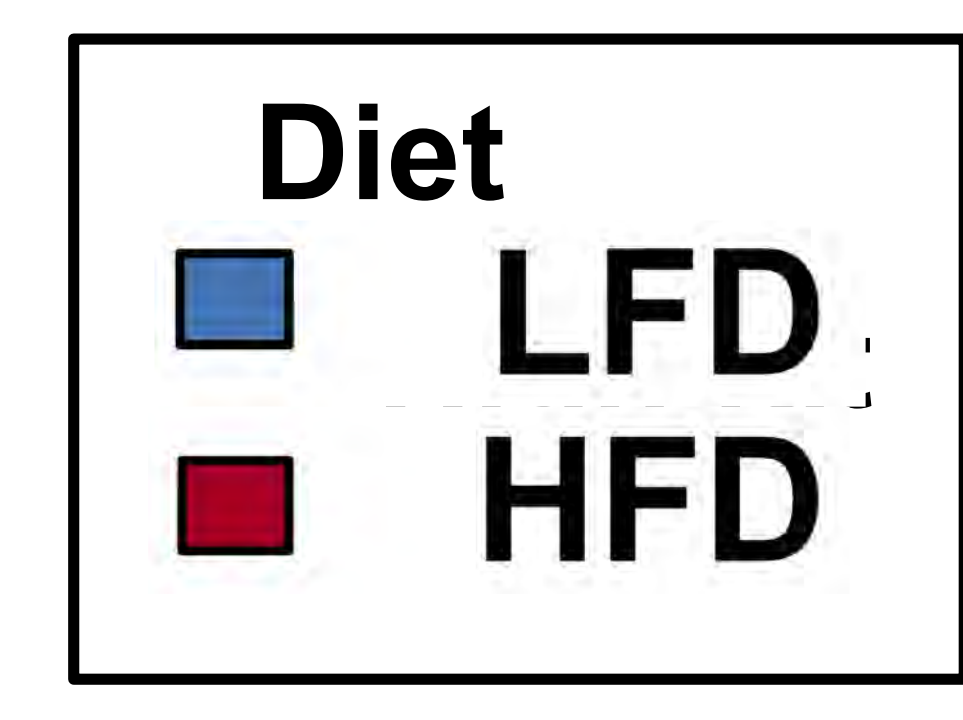
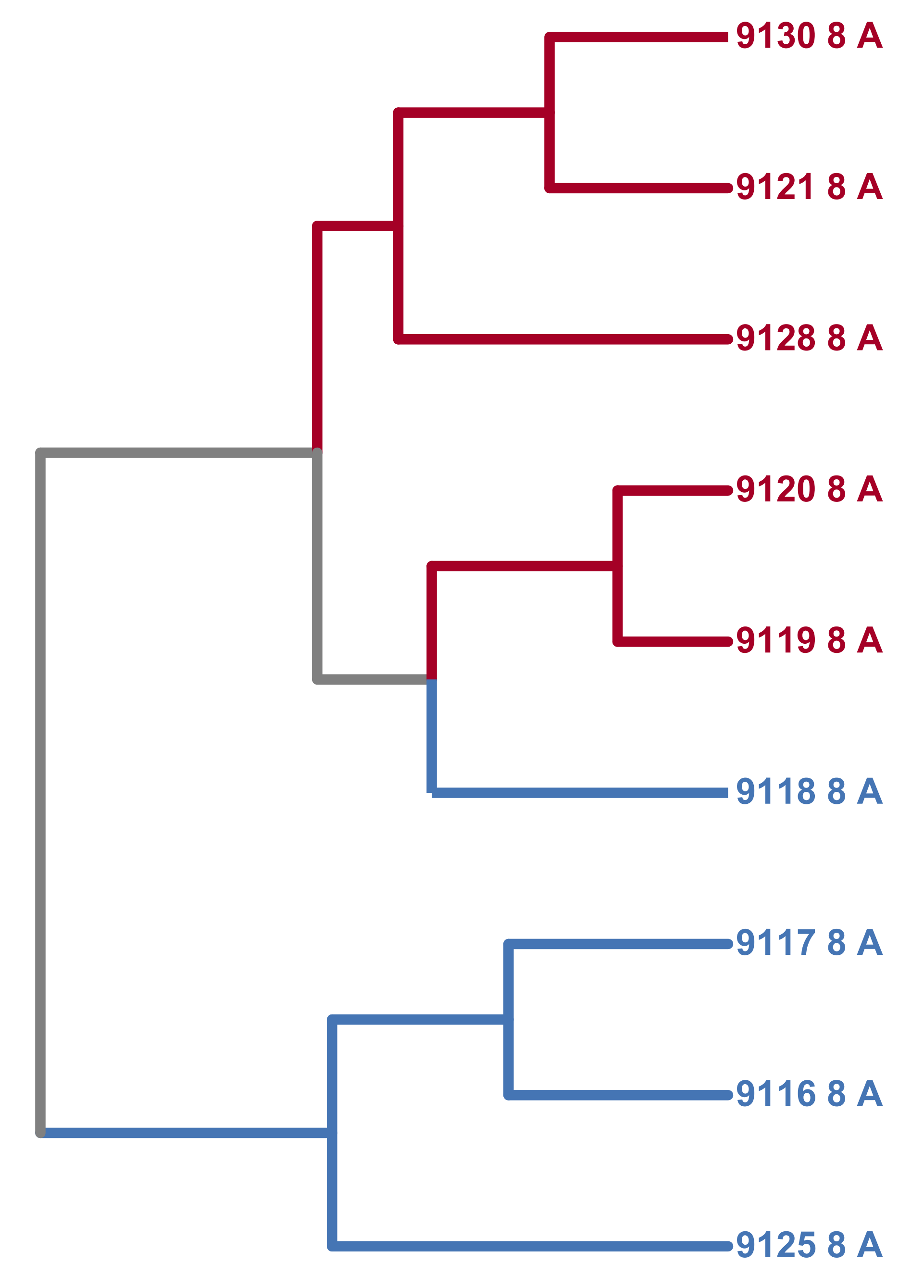


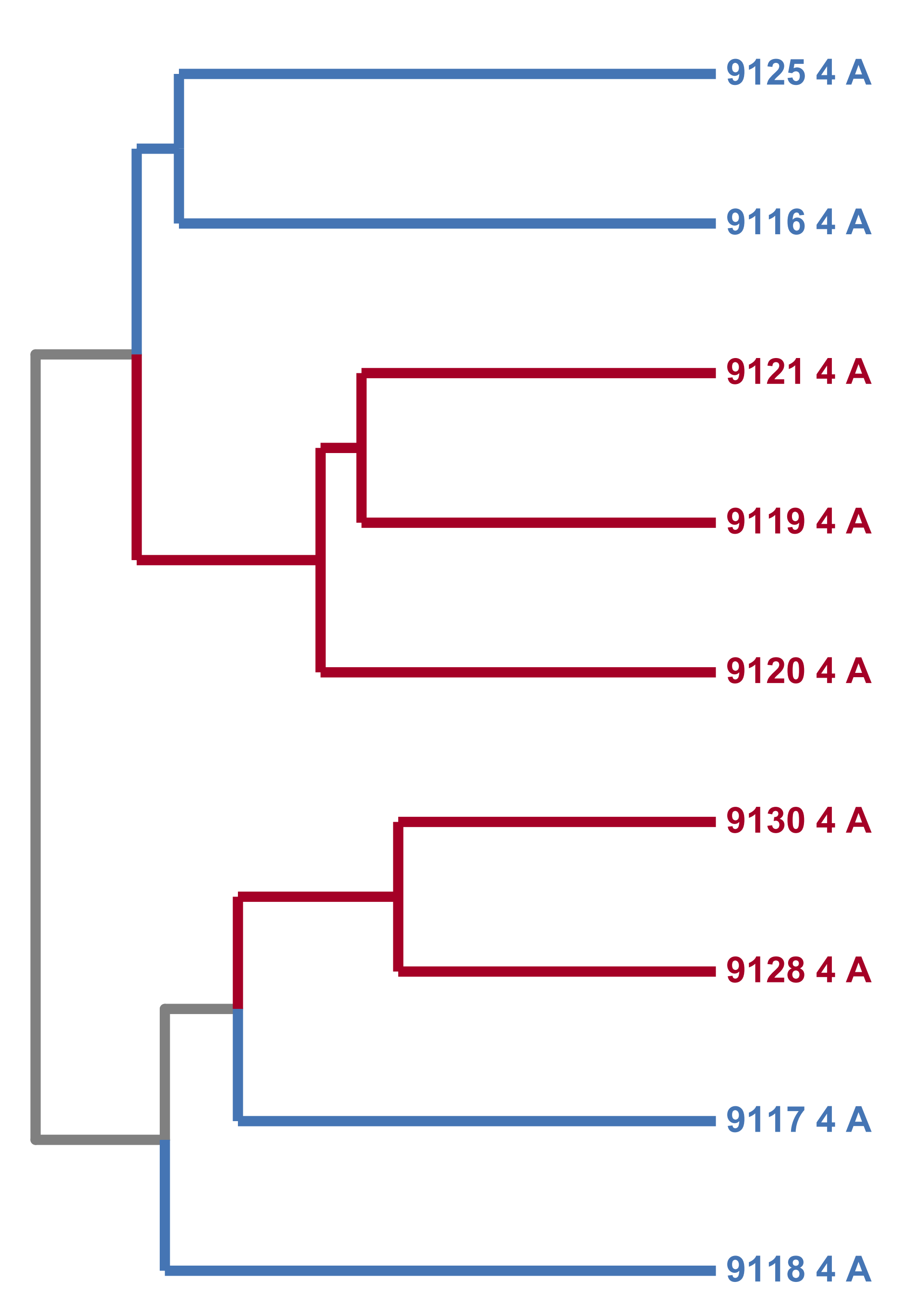
Figure 2

A

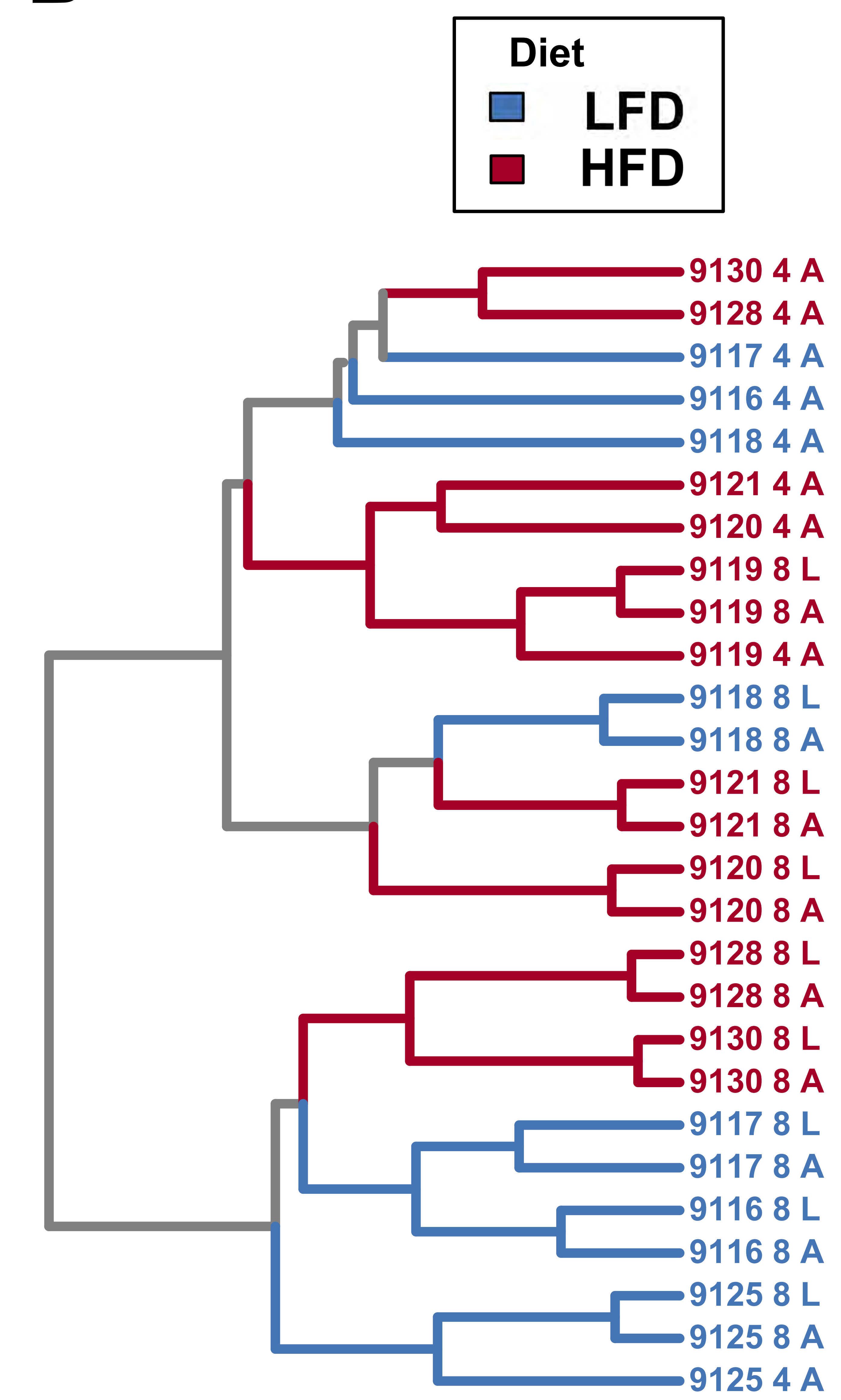
CD8 T cells



CD4 T cells



B



C

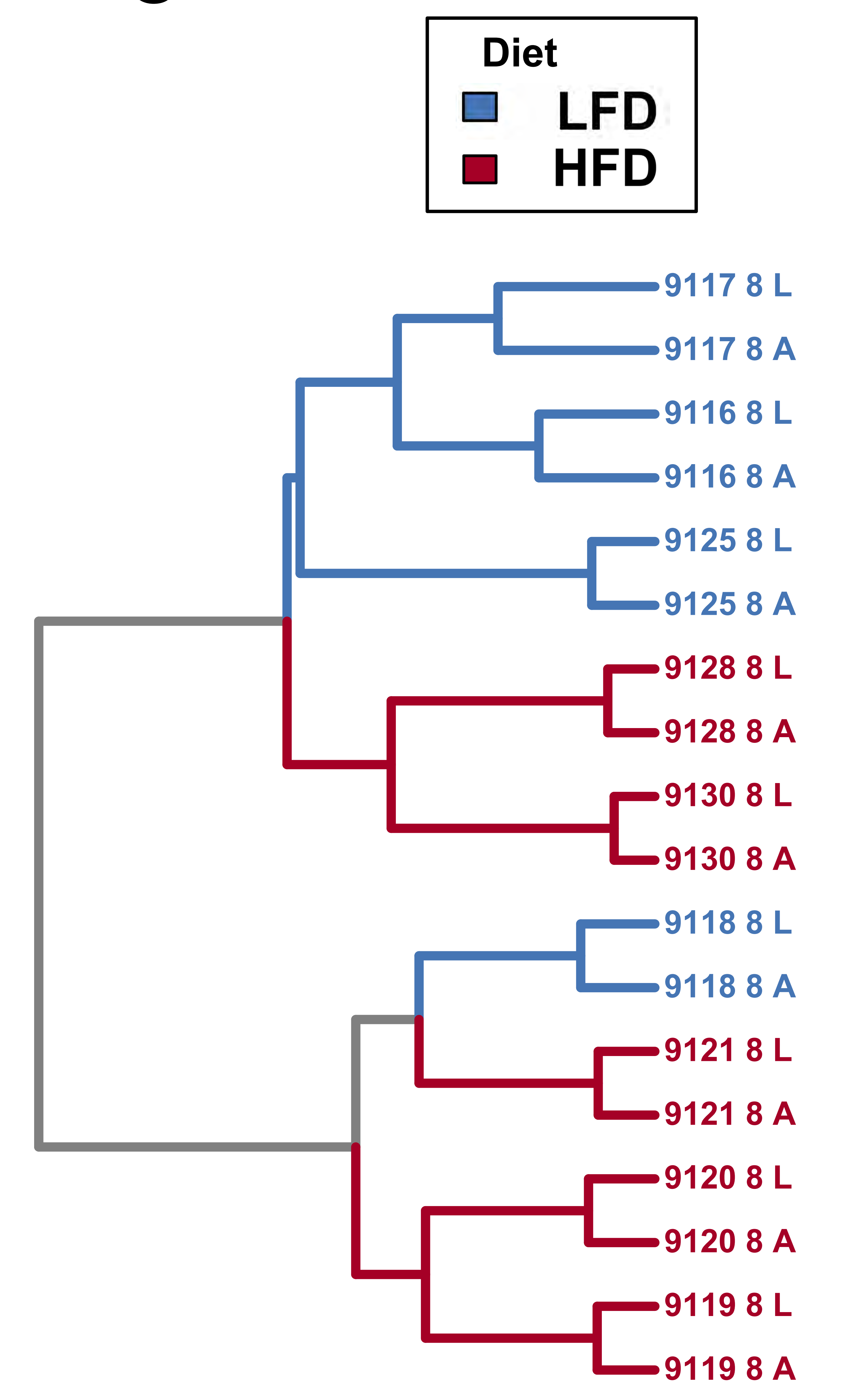
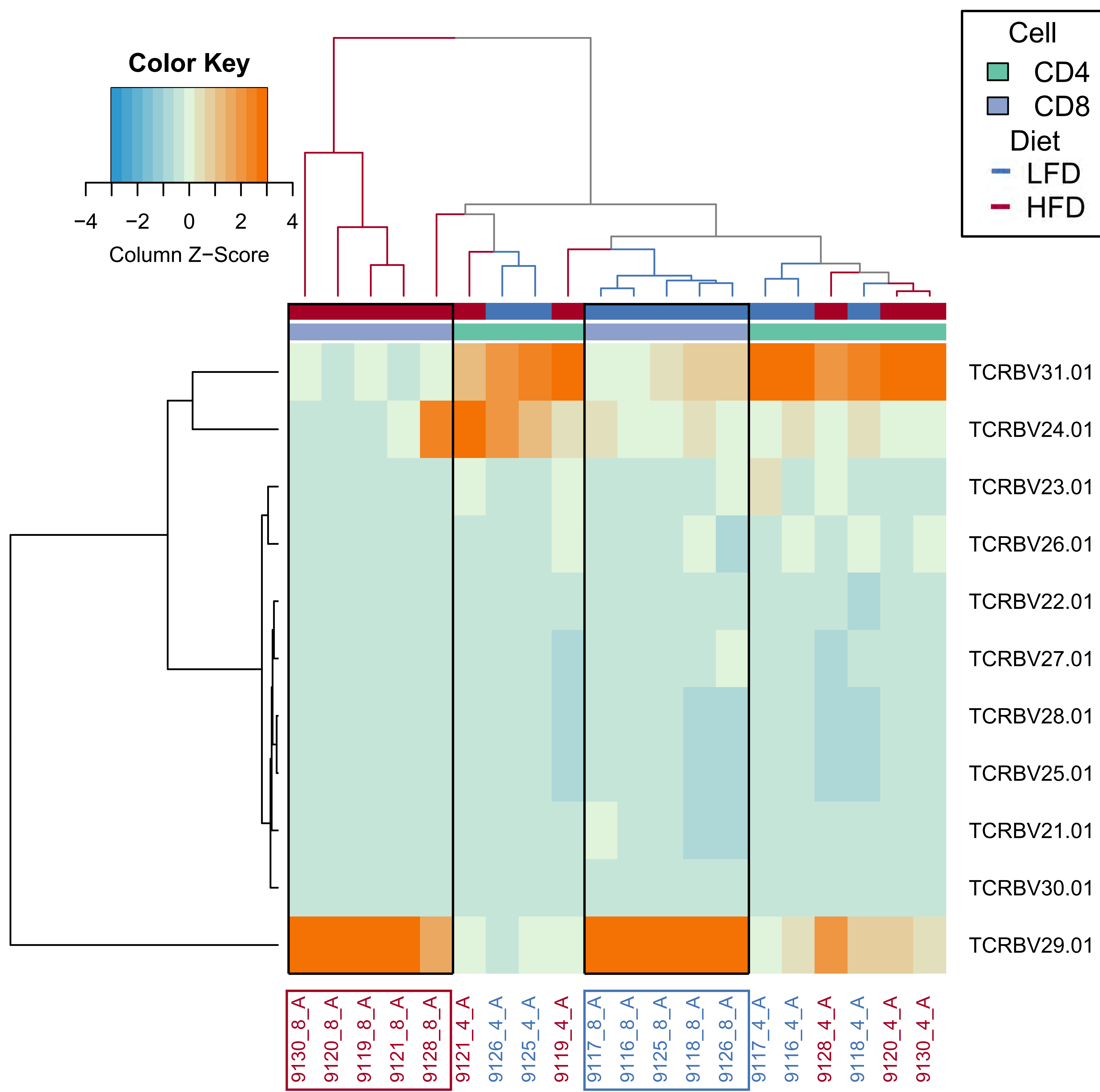


Figure 3

A



B

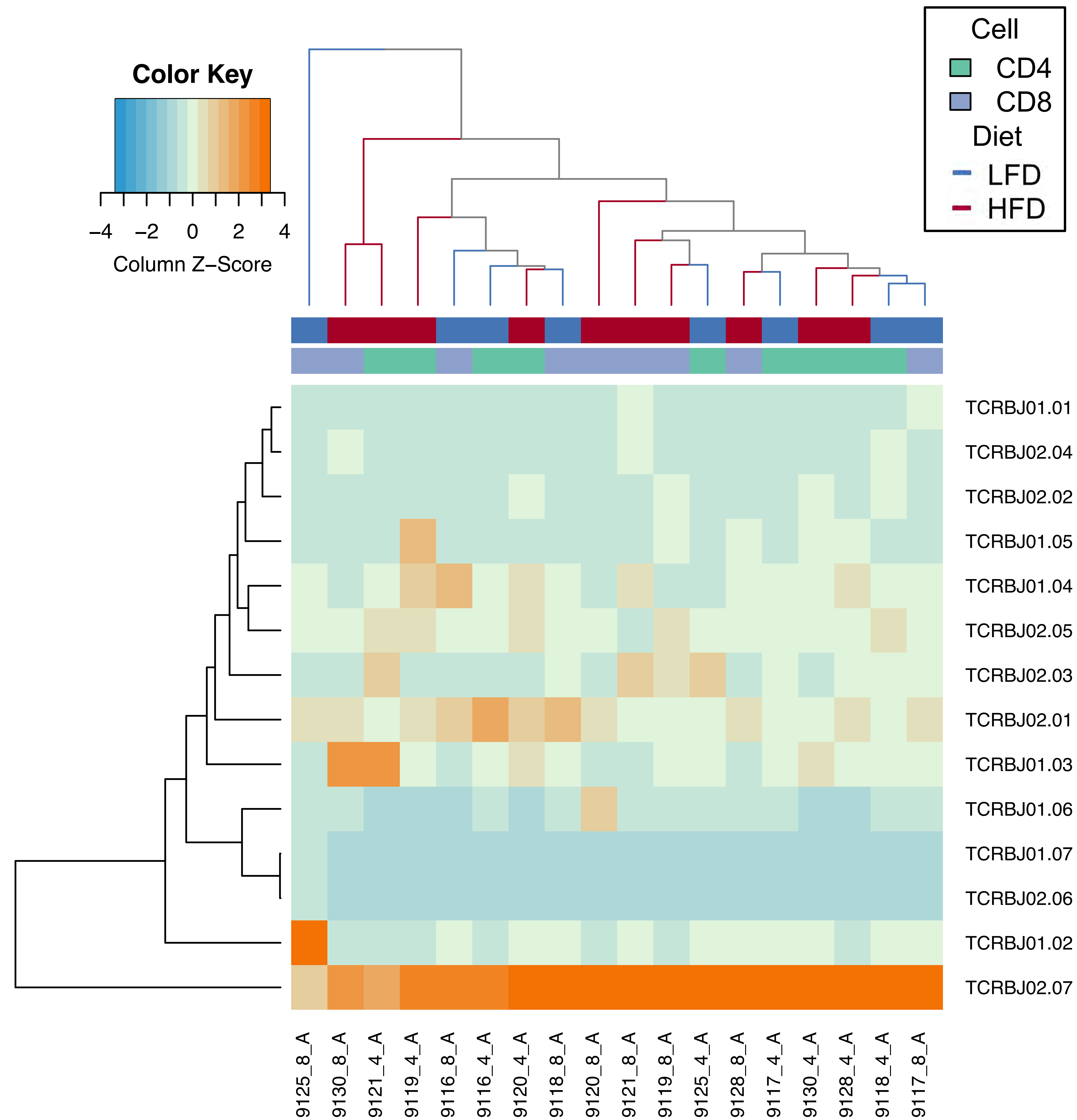


Figure 4

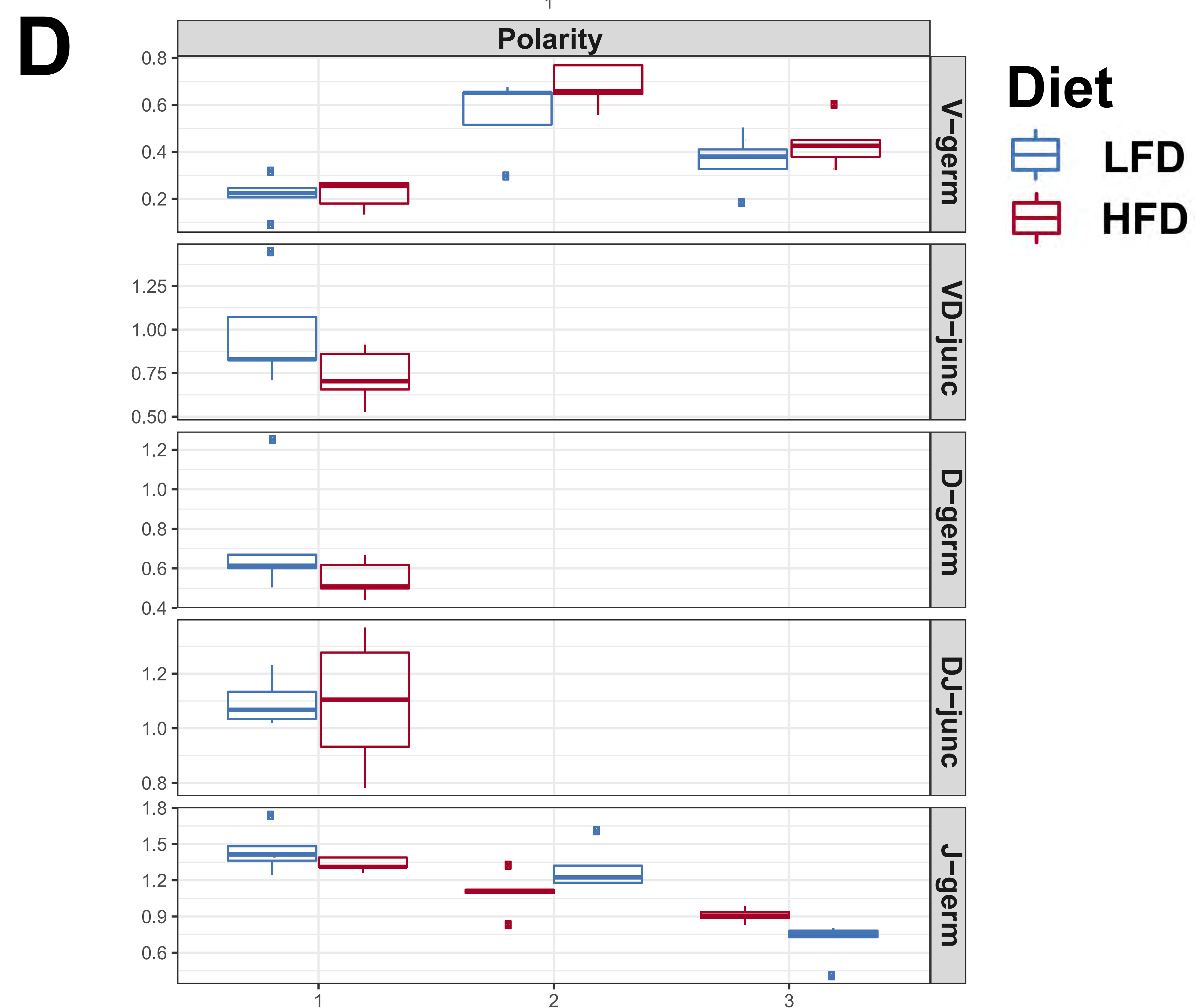
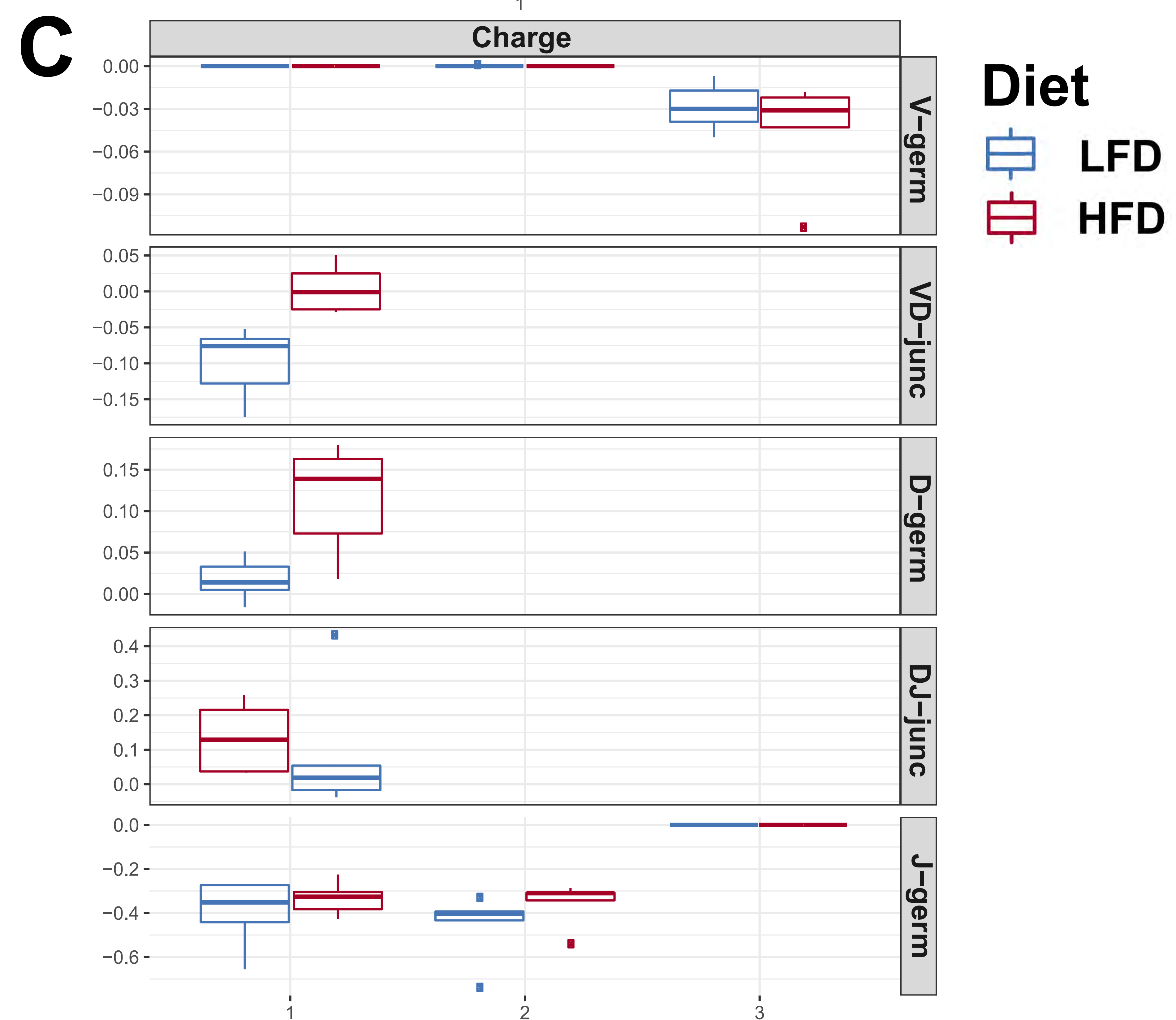
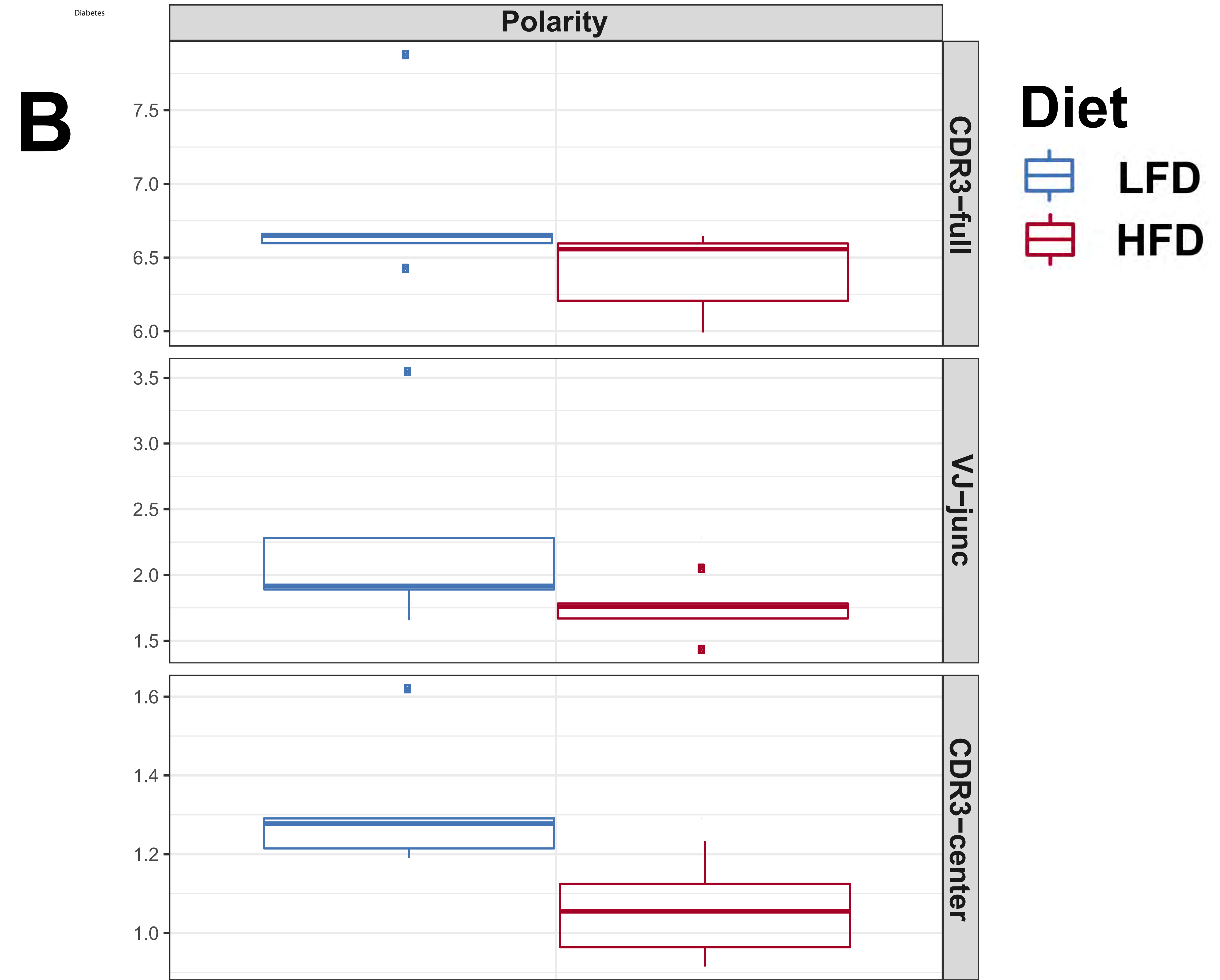
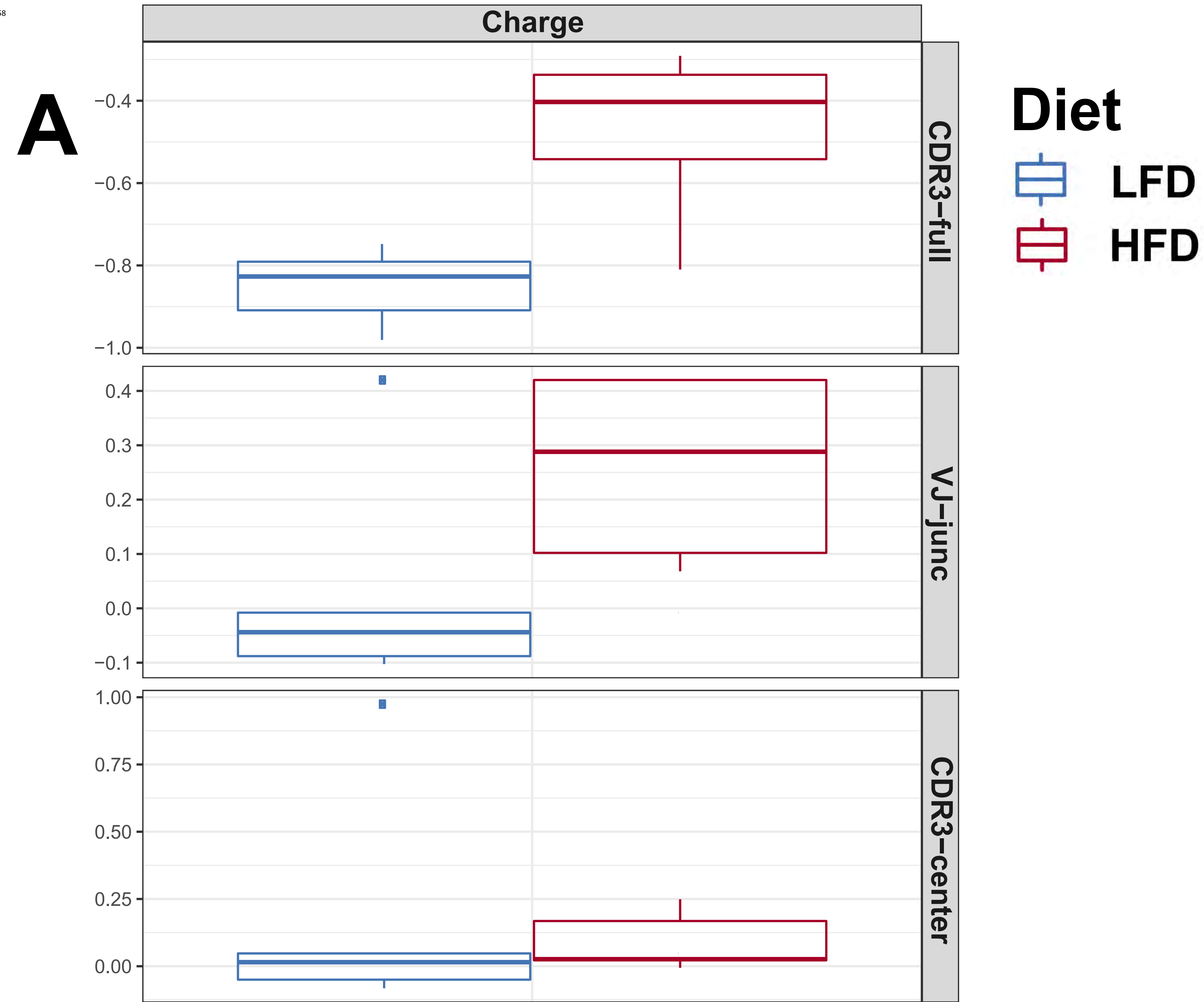


Figure 5

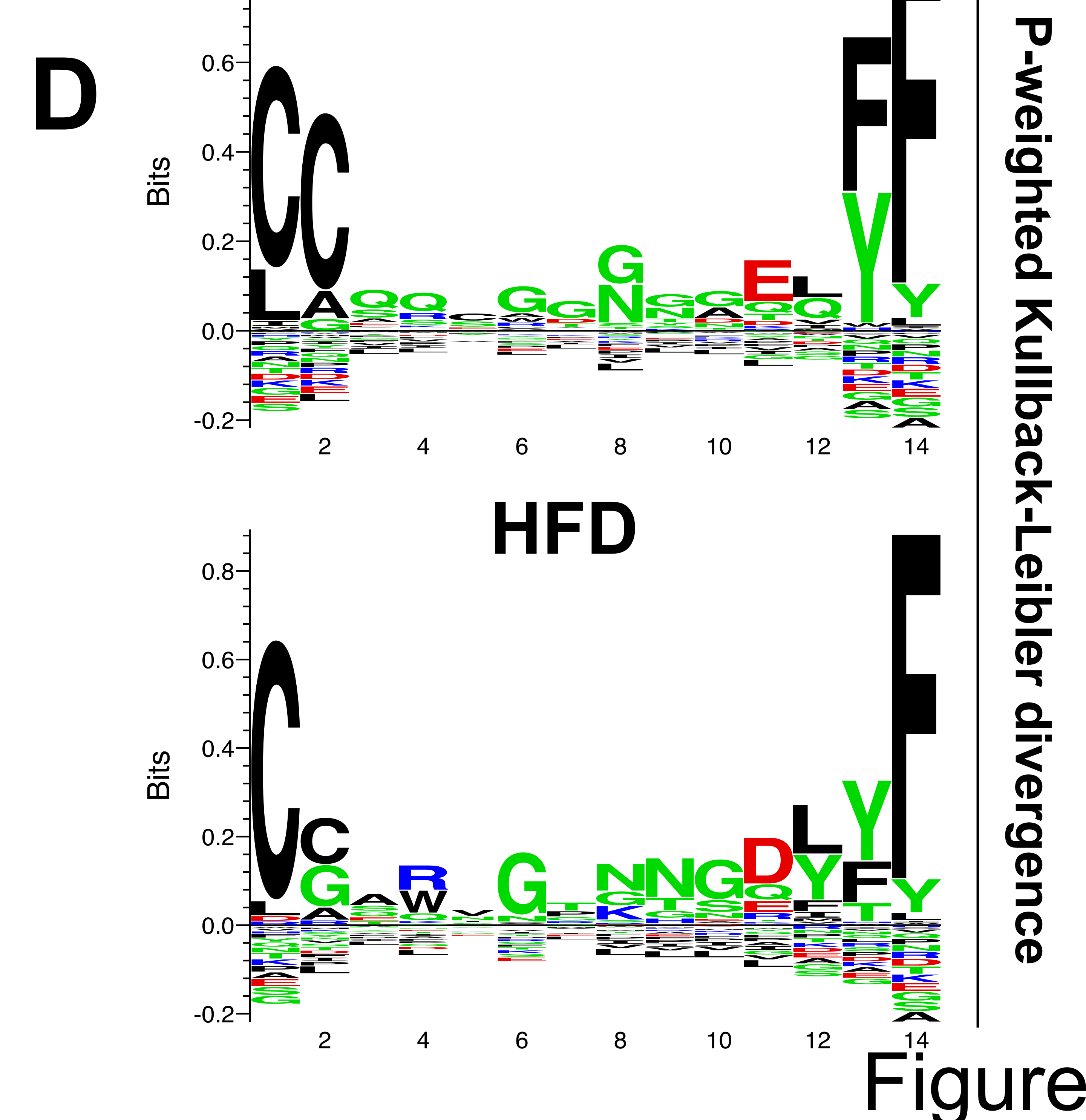
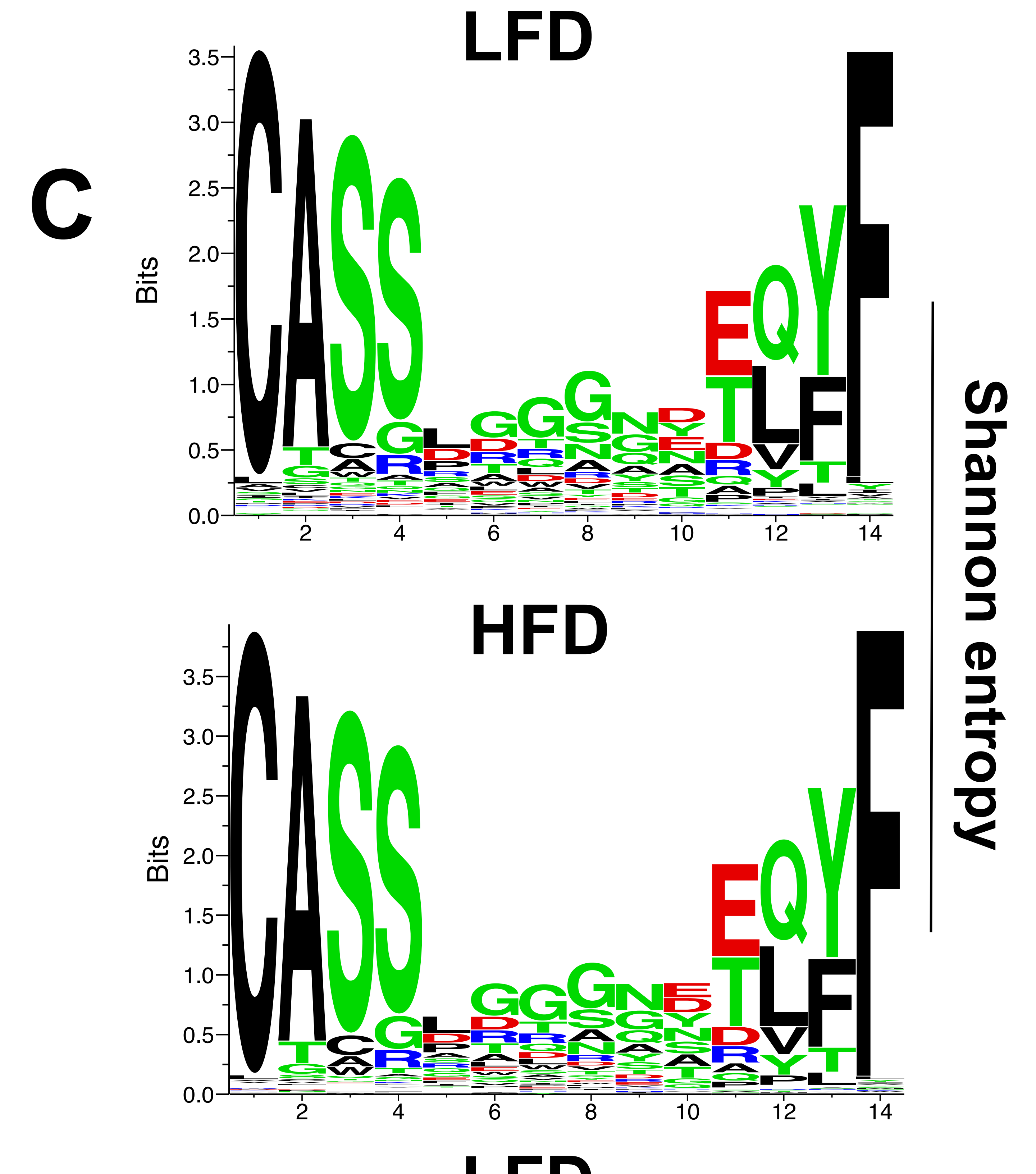
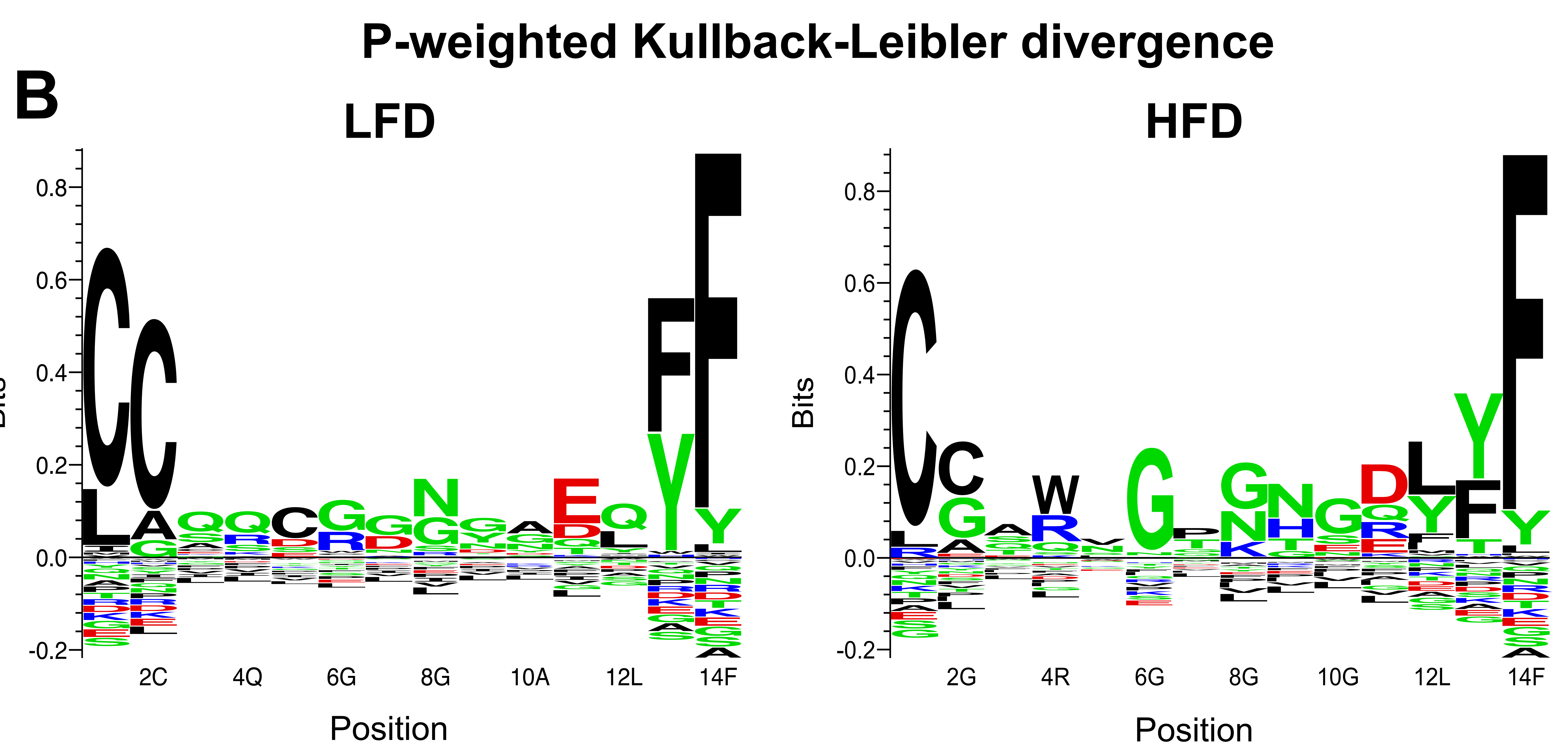
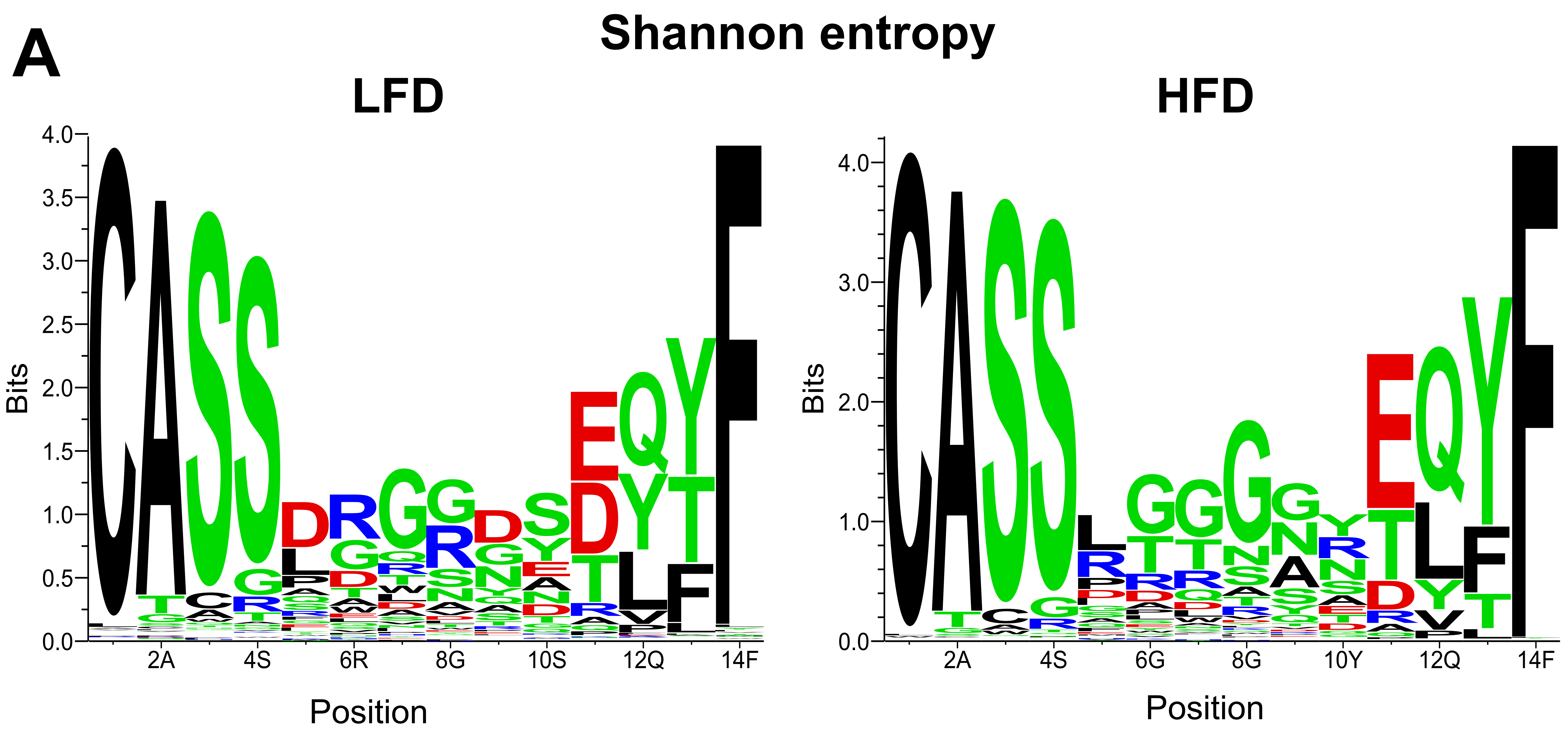
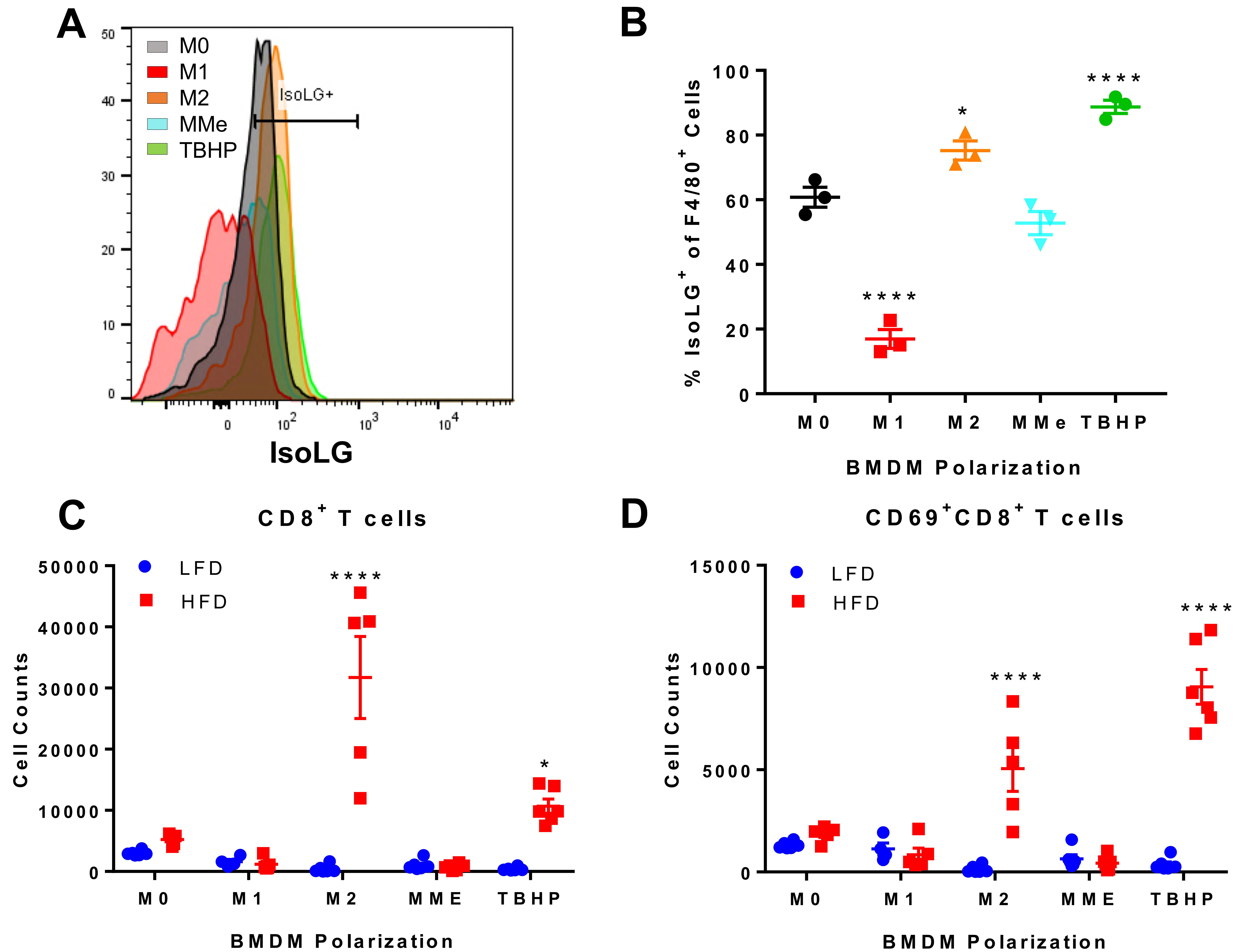


Figure 6



Supplementary Information (1). Shared clonotypes between and within dietary groups by cell and tissue type. The data is available at

<https://dx.doi.org/10.6084/m9.figshare.6752834>

Supplementary Table 1. Descriptive statistics of how many of the top 50 and top 10 clonotypes are shared between the CD8⁺ TCR repertoires of AT and liver.

Figure S1. Gating strategy for AT T cells.

Figure S2. (A) Gating Strategy for total ATMs and (B) quantification of ATMs in LFD and HFD mice. (B) ATMs are significantly higher in diet-induced obesity. (C) Gating strategy for CD11c and CD206 expressing ATMs and quantification of flow analysis.

Figure S3. Gating strategy for polarized BMDMs.

Figure S4. Gating strategy for T cells co-cultured with polarized BMDMs.

Figure S5. Male C57BL/6J mice were placed on a 10% low-fat diet (LFD) or a 60% high-fat diet (HFD) as described in the Methods. (A) Mice on HFD demonstrated a significant increase in body weight, (B) epididymal AT weight, and (C) liver weight (one-way ANOVA with Bonferroni correction). (D) Fasting blood glucose did not differ between the groups (one-way ANOVA with Bonferroni correction). (E) Plasma insulin concentrations were elevated in the HFD mice (one-way ANOVA with Bonferroni

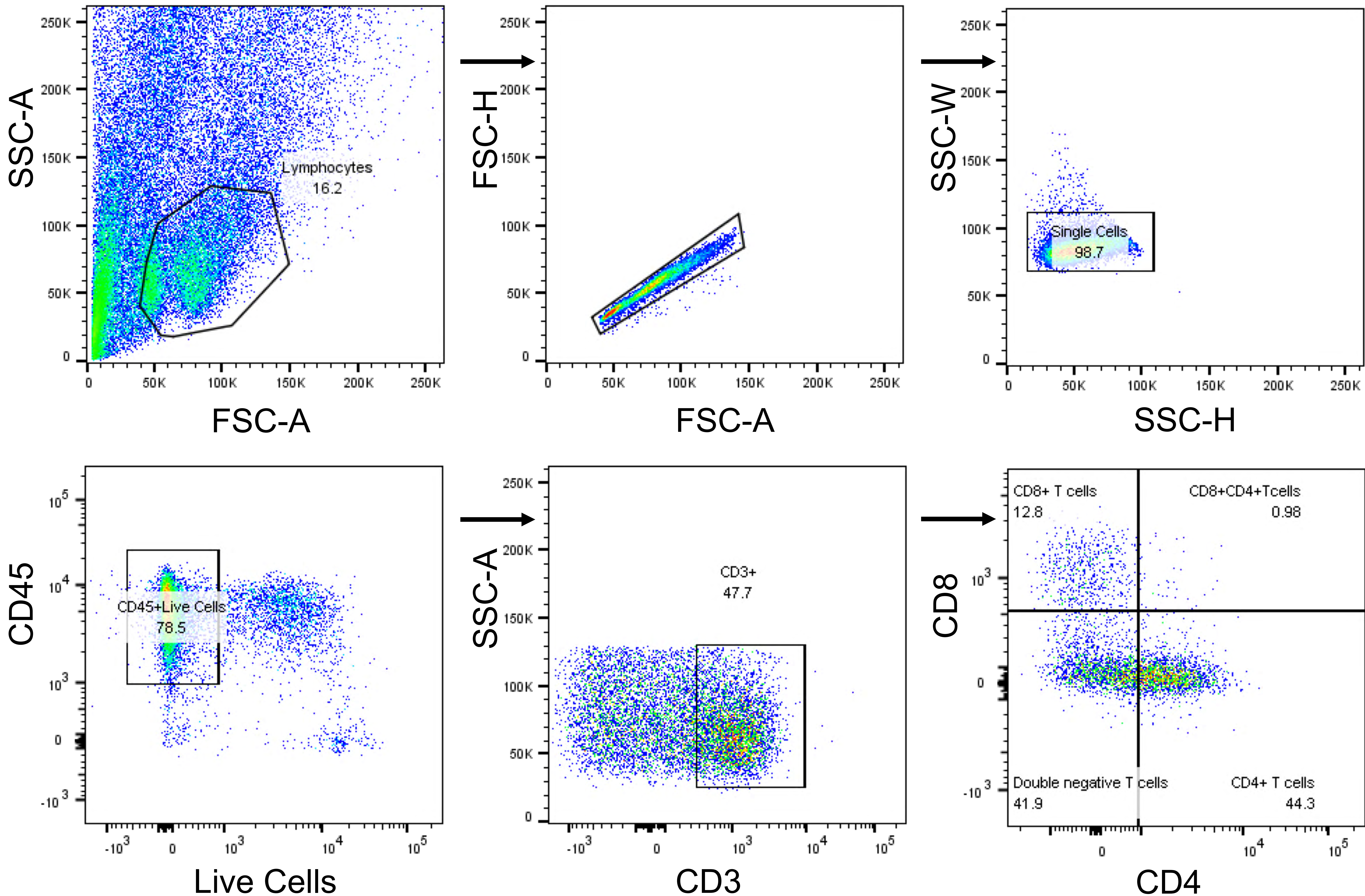
correction). **(F)** Glucose tolerance testing revealed that the glucose tolerance of HFD-fed mice was significantly impaired (two-way ANOVA with *post-hoc* Bonferroni-Šídák multiple comparisons testing). Data are presented as mean \pm SEM, n = 4-5 mice/group.

Figure S6. Hierarchical clustering using geometric mean overlap reveals that CD4⁺ and CD8⁺ repertoires possess characteristically unique sets of TCRs, and that these repertoires are distinct in multidimensional space.

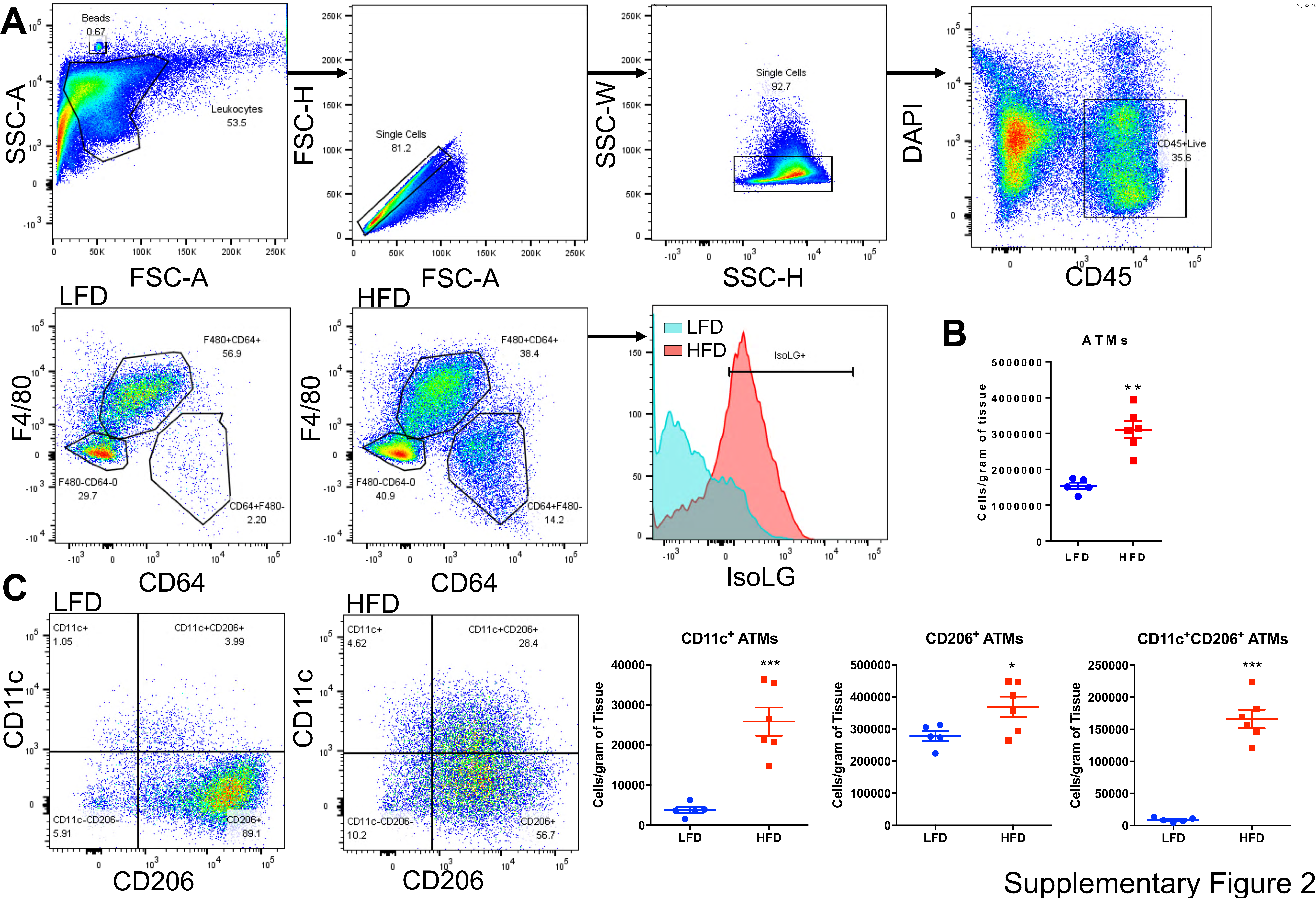
Figure S7. CD4⁺ TCR repertoires utilize CDR3s with decreased charge and polarity in comparison to CD8⁺ TCR repertoires ($P < 0.05$, Wilcoxon signed-rank test). N(D)N length of CD8 and CD4 T cells ($P < 0.05$, Wilcoxon signed-rank test).

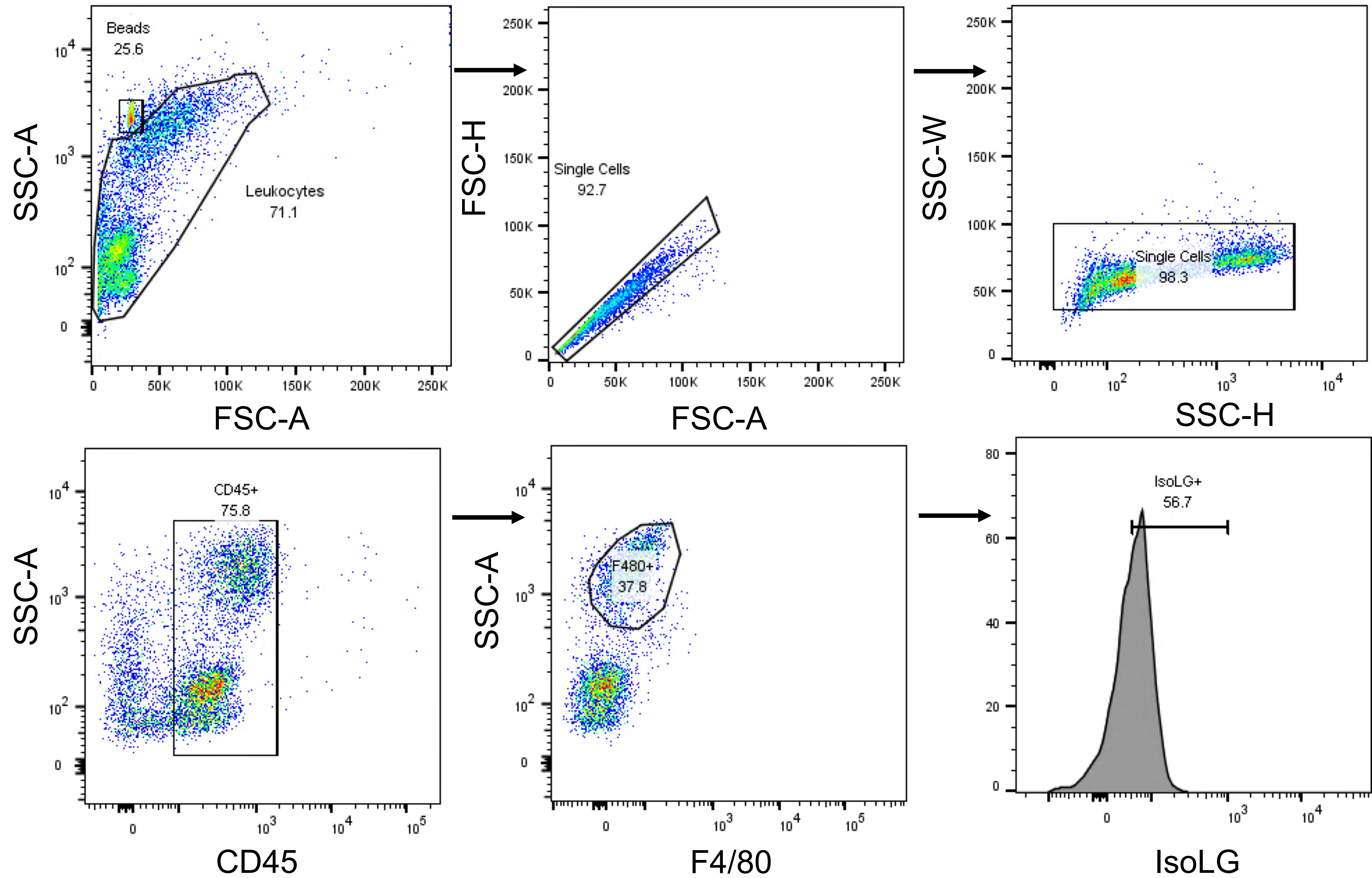
Figure S8. Calculation of repertoire publicity measure. **(A)** Each TCR is counted as present or absent within a given sample. **(B)** A contingency table is built by counting whether a given TCR is predominantly present within a treatment group (1), equally present between treatment groups (0), or present within the other treatment group (0). **(C)** Contingency table testing is performed to evaluate the null hypothesis that public clonotypes are evenly distributed between treatment groups. Either Pearson's χ^2 test or the Barnard test are appropriate to implement, though Fisher's exact test is not recommended due to its requirement that marginals of the contingency table remain equal. If Pearson's χ^2 test is used, Monte Carlo simulation should be used to ensure that the P-value observed would still be considered significant within the probability null distribution.

Mouse	Low-fat diet					High-fat diet				
	16	17	18	25	26	19	20	21	28	30
# clones shared between top 50	25	19	36	18	18	29	22	32	29	33
# clones shared between top 10	9	5	9	8	8	9	8	9	9	10

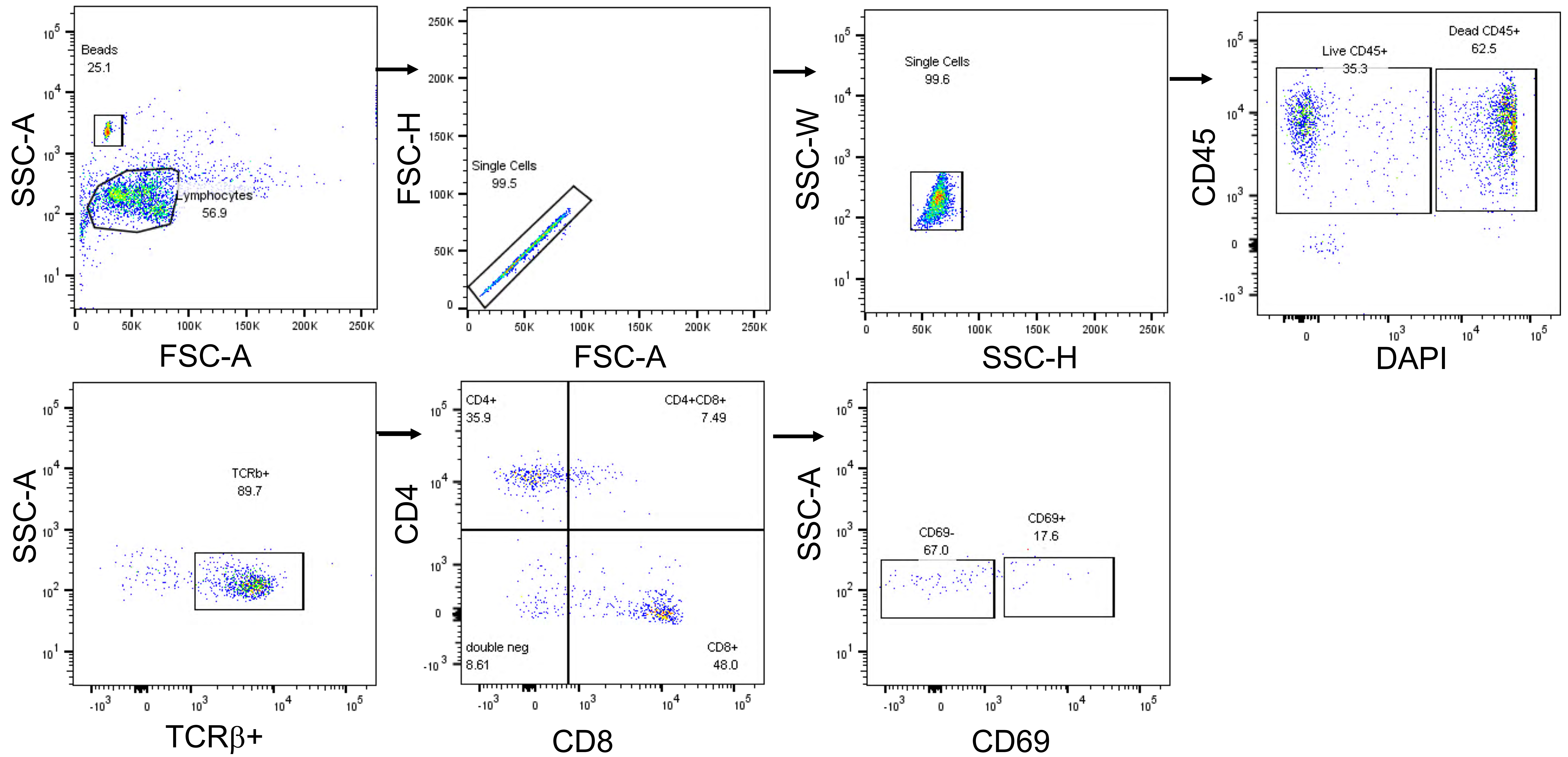


Supplementary Figure 1

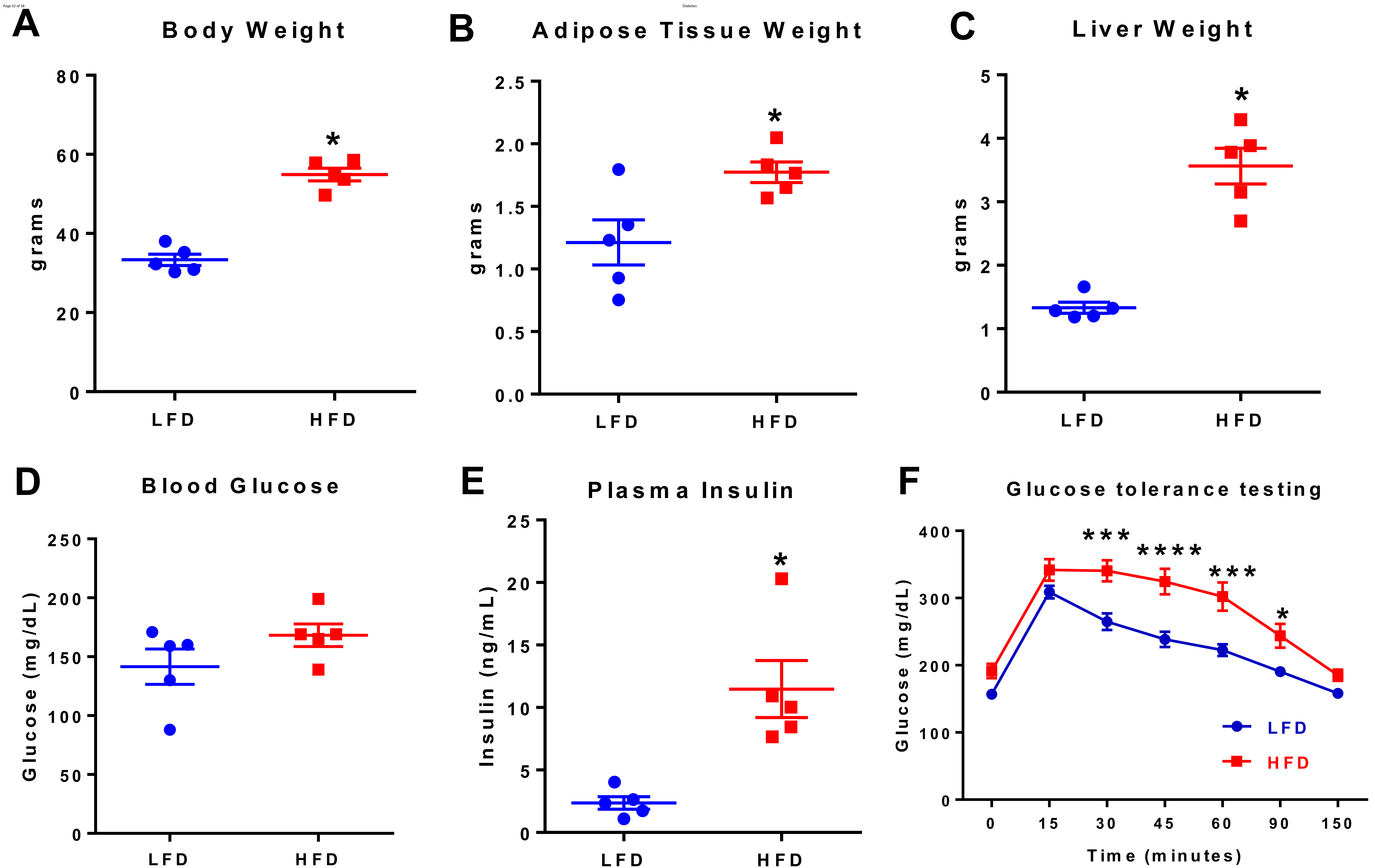




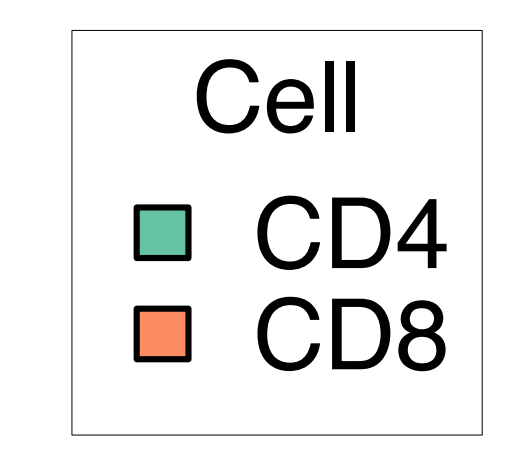
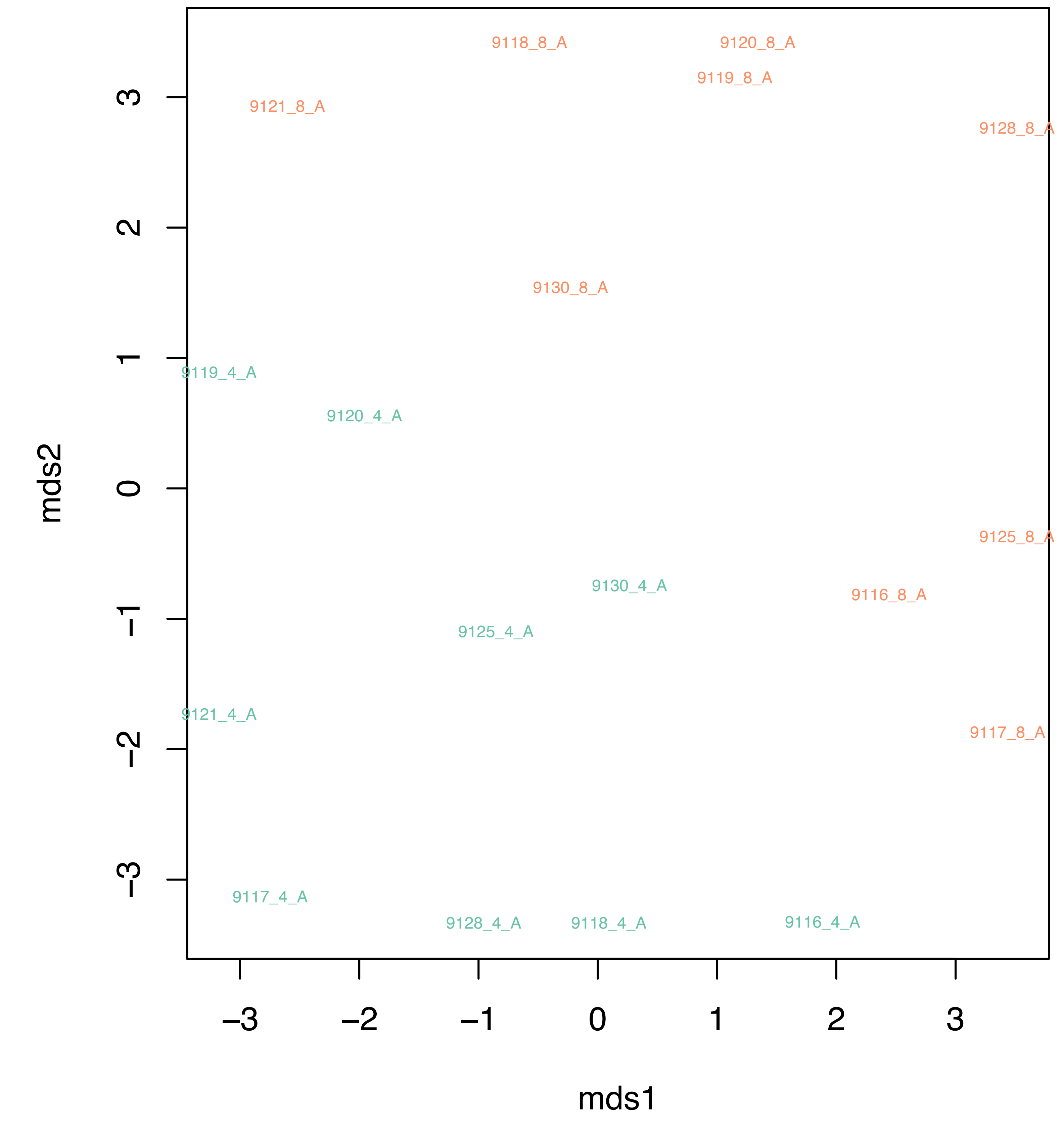
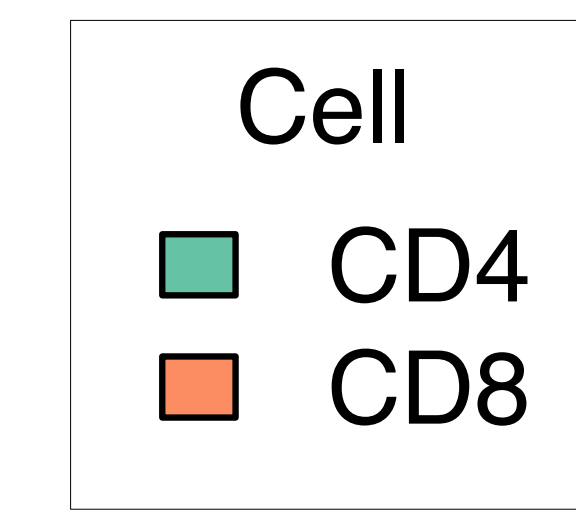
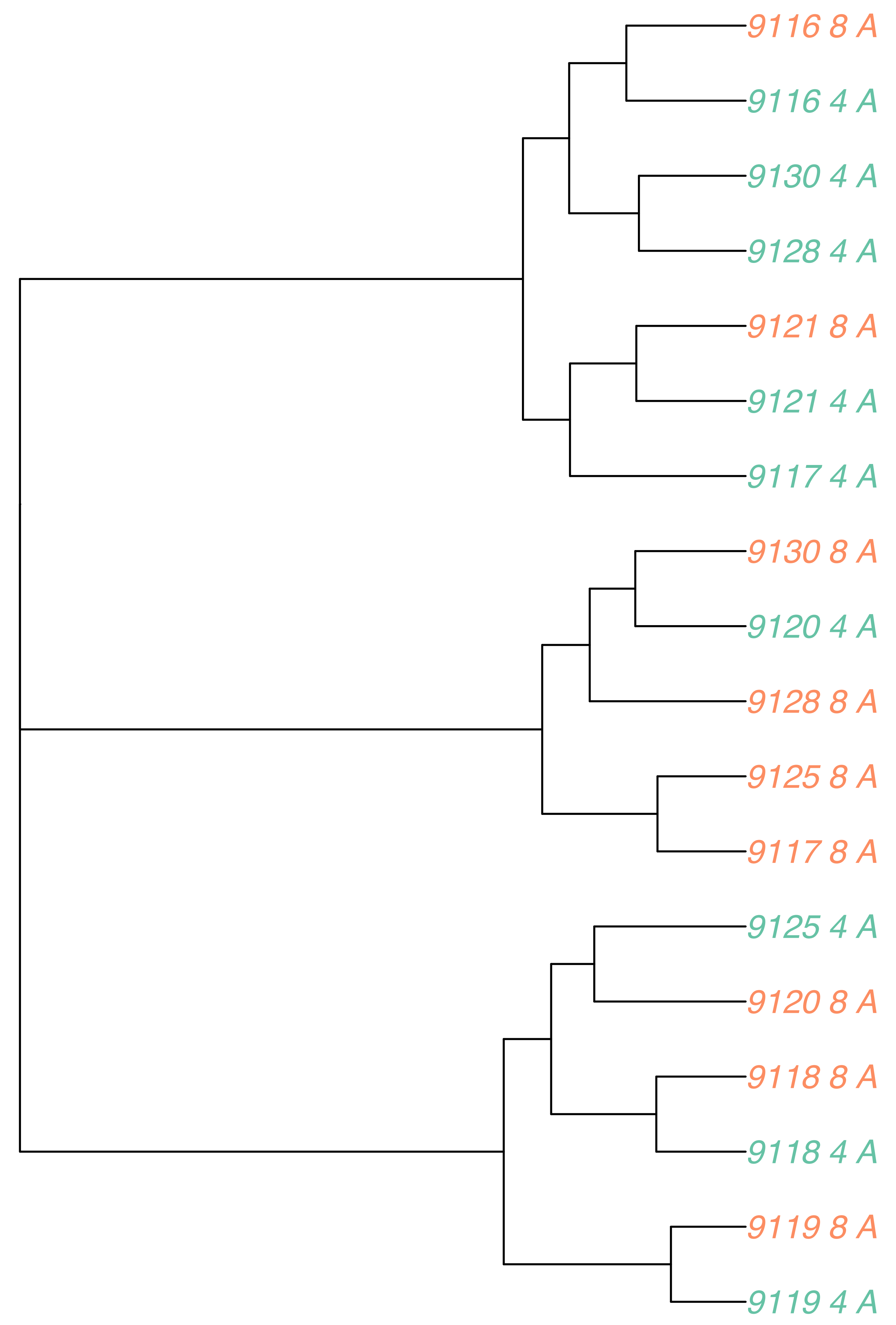
Supplementary Figure 3



Supplementary Figure 4

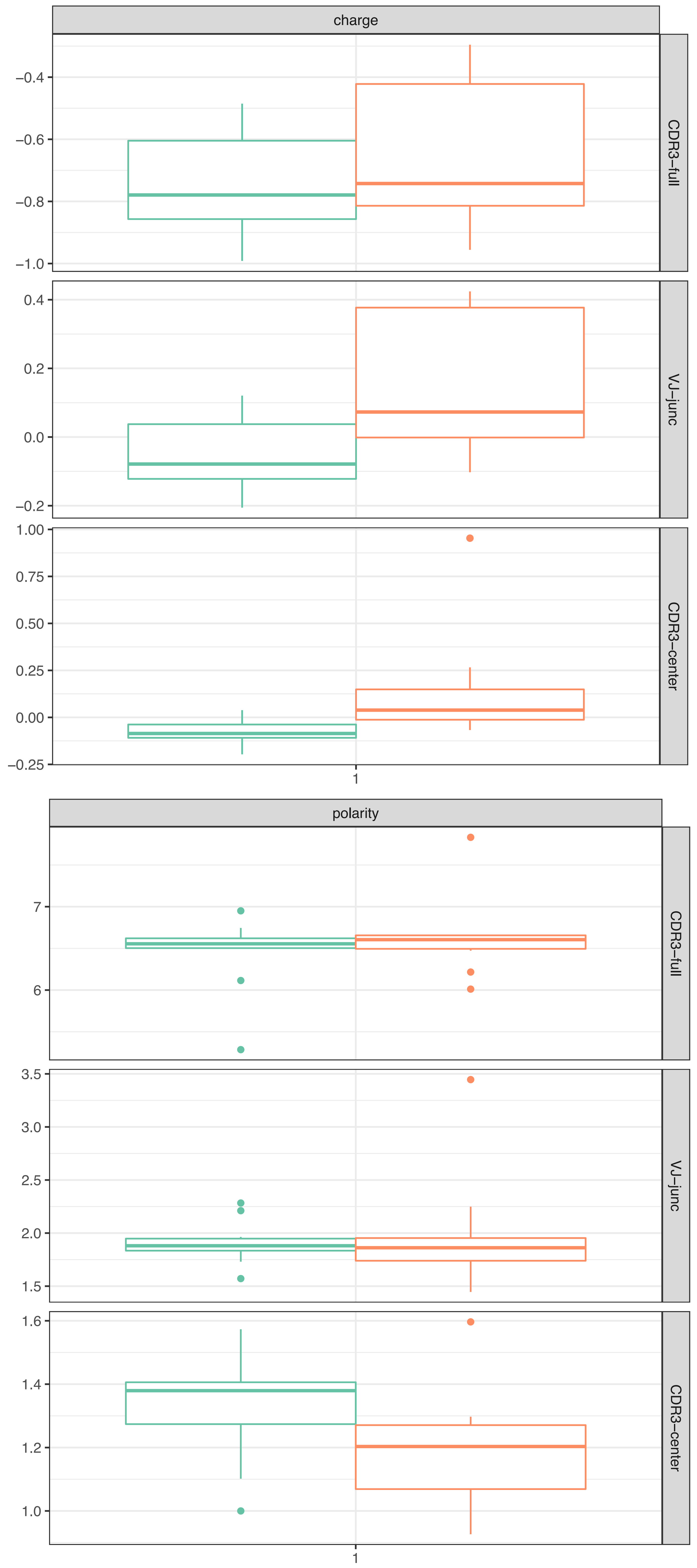
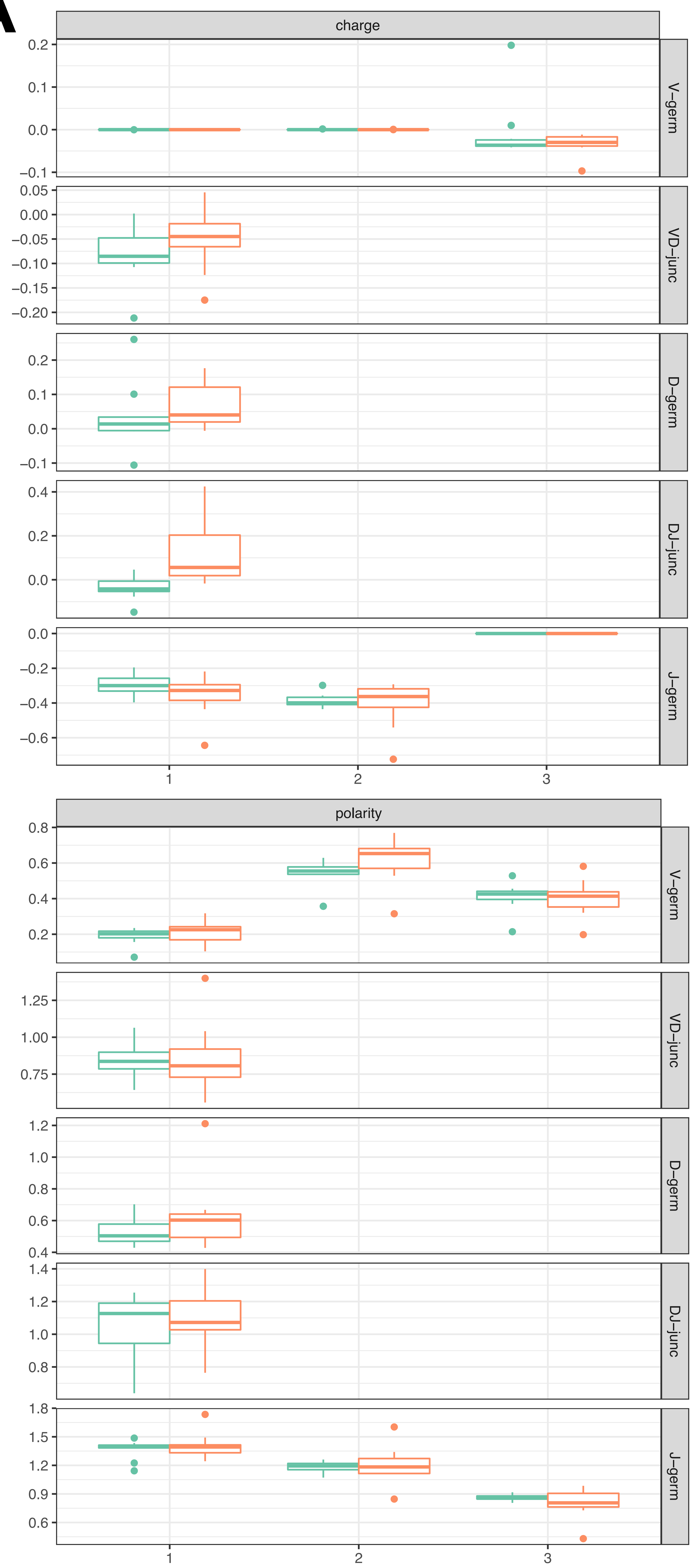


Supplementary Figure 5



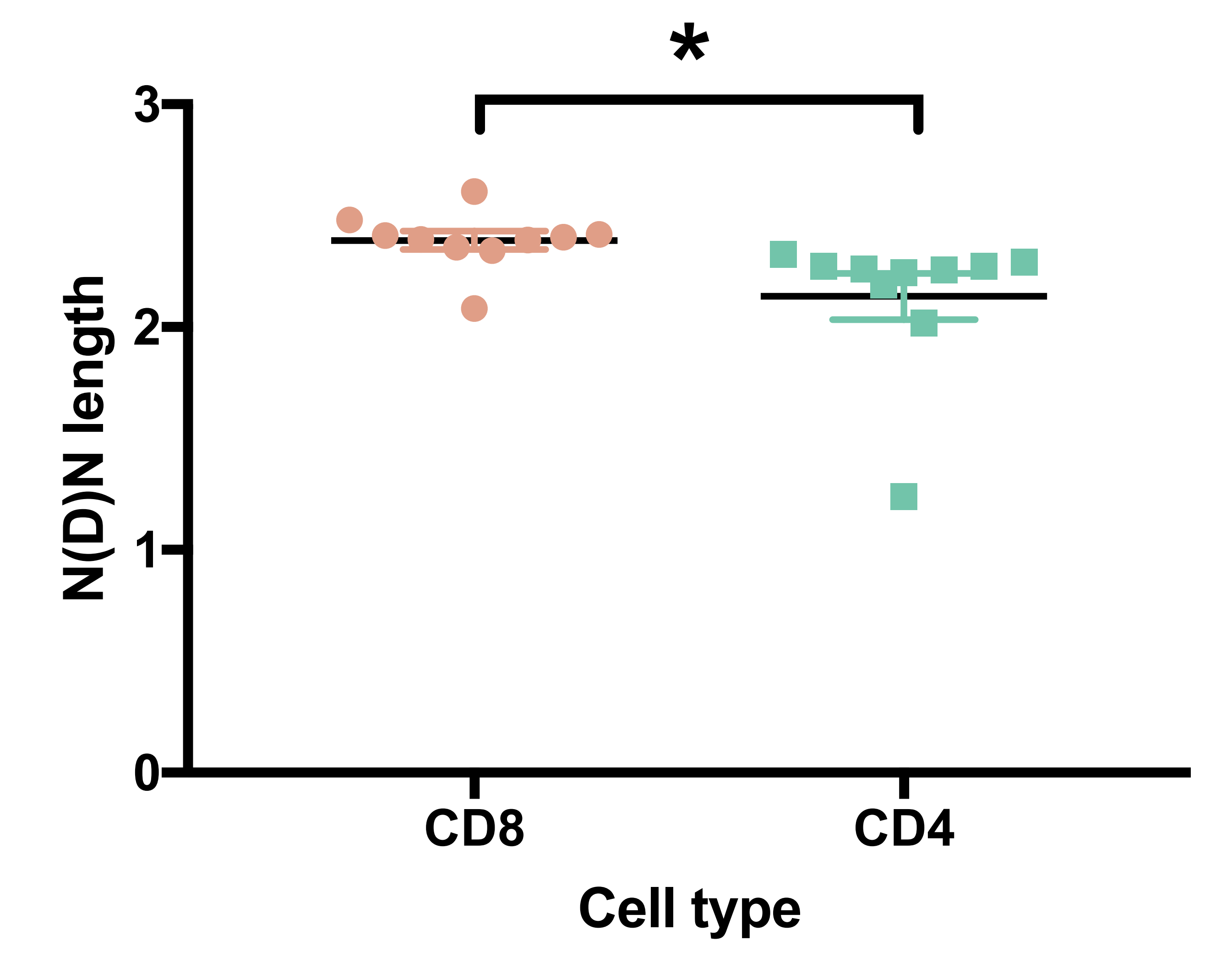
Supplementary Figure 6

A



B

Longer N(D)N length of CD8 T cells



A

For each treatment group:

$$\sum_{j=1}^m \left[\sum_{i=1}^n TCR_{ij} > 0 \right]$$

**B**

Contingency table summarizing skewness of clones:

$$\begin{bmatrix} \text{Active}_{greater} & \text{Inactive}_{greater} \\ \text{Active}_{lessequal} & \text{Inactive}_{lessequal} \end{bmatrix} \quad \begin{bmatrix} 10 & 4 \\ 11 & 17 \end{bmatrix}$$

**C** χ^2 test on contingency table**D**Pearson's χ^2 P value: 0.04953Monte Carlo simulated P value: 0.07892Barnard's test P value: 0.055904 (2-sided)